Poly-(amino acid) polyelectrolyte films: Structure and interactions with proteins and lipids

PhD Thesis

Ana-Maria Pilbat

Supervisor
Balázs Szalontai

Institute of Biophysics
Biological Research Centre
Hungarian Academy of Sciences
Szeged, Hungary

2008

Table of Contents:

Acknowledgements

This thesis is the fruit of work in the Institute of Biophysics, Biological Research Centre, Hungarian Academy of Sciences. Here, I would like to acknowledge for people, who helped me in my work and for my friends who made my stay in Szeged a delight.

First of all, I would like to express my warmest gratitude to my supervisor Dr. Szalontai Balázs, who introduced me into the fascinating biophysical world, who was a constant source of support and advancing during my ITC and PhD, for his careful mentoring at the crucial moments and for his uninterrupted presence and his well intentioned advice saved me many times from difficulties.

I am greatly indebted to Prof. Pál Ormos, head of the Institute and for Dr. Páli Tibor head of the Membrane Structure and Dynamics group, for providing me with the opportunity to work at the Institute.

I would like to express many thanks to my college, Dr. Kóta Zoltán for his guidance of my work, for inspiring ideas, useful advices and critics.

Special thanks go to my parents for their support, understanding and love, and to all of my friends who were with me during this period. Especially to Dr. Bálint Zoltán, who always showed me the good way, to Ferencz Csilla-Mária and Verebes Beáta for their support.

Papers related to the thesis

1. **A-M. Pilbat**, V. Ball, P. Schaaf, J. Voegel, B. Szalontai
   Partial Poly(glutamic acid) ↔ Poly(aspartic acid) Exchange in Layer-by-Layer Polyelectrolyte Films. Structural Alterations in the Three-Component Architectures.
   Langmuir 22, 5753-5759 (2006).

2. **A-M. Pilbat**, Z. Szegletes, Z. Kota, V. Ball, P. Schaaf, J. Voegel, B. Szalontai
   Phospholipid Bilayers as Biomembrane-like Barriers in Layer-by-Layer Polyelectrolyte Films.
   Langmuir 23, 8236-8242 (2007).

List of Abbreviations

AC mode	**alternative contact mode**
AFM	**atomic force microscope**
α-MSH	**alpha-melanocyte stimulating hormone**
ATR	**attenuated total reflection**
D_2O	**heavy water**
DMPC	**dimyristoylphophatidylcholine**
DPPC	**dipalmitoylphosphatidylcholine**
FTIR	**Fourier-transform infrared**
GRA	**gramicidin a**
HSA	**human serum albumin**
LBL	**layer-by-layer**
PAA	**poly(L-aspartic acid)**
PAH	**poly(allylaminehydrochloride)**
PEI	**poly(ethyleneimine)**
PGA	**poly(L-glutamic acid)**
PLL	**poly(L-lysine)**
PSS	**poly(sodium 4-styrenesulfonate)**
SVD	**singular value decomposition**

Introduction

Many medical and analytical devices use different kind of materials such as synthetic polymers, ceramics, metals, biological derivate substances and composites. These materials have been selected on the basis of their physical or/and mechanical properties rather than their biological performance. Materials of synthetic or natural origin in contact with biological fluid differ from application to application; the accepted universal requirement is biocompatibility. Biocompatibility can be described like the “ability of a material to perform with an appropriate host response in a specific application” Williams definition [1].

This is a simple, and clear definition, but as time passed, and our knowledge increased, the definition became more complex: Biocompatibility "refers to the ability of a biomaterial to perform its desired function with respect to a medical therapy, without eliciting any undesirable local or systemic effects in the recipient or beneficiary of that therapy, but generating the most appropriate beneficial cellular or tissue response in that specific situation, and optimising the clinically relevant performance of that therapy" [2]. The increase of the complexity of the definition in the last nine years well illustrates the speed of the progress in this field.

The goals of the present work are more in line with the first definition. Firstly, we intended to understand basic phenomena concerning the organisation and structure of polyelectrolyte films made from polyaminoacids; secondly, we wanted to explore the experimental possibilities to create artificial systems, which might later serve as bases for practical applications.

In this thesis, we present data concerning the structure and internal interactions of polypeptide multilayers. We also present the first studies on phospholipid bilayers incorporated into polypeptide multilayers. Due to their close resemblance to real biological systems, these bilayers on the cytoskeleton-like polypeptide films may serve as internal barriers, as carriers of hydrophobic proteins, which might have desirable biological functions (ion channels, transporters, etc.). Finally, preliminary data are presented on the possibility of biomedical use of such lipid bilayers in connection with polyelectrolyte films.

1. Literature

1.1. Why polyelectrolyte films?

Multilayered polyelectrolyte films prepared by the layer-by-layer (LBL) consecutive adsorption method [3] became very popular in the past decade because of the numerous possible applications of this approach in various fields. Applications could be said to fall into two general categories, tailoring interactions of a surface with its environment and fabricating "devices" with defined structural properties.

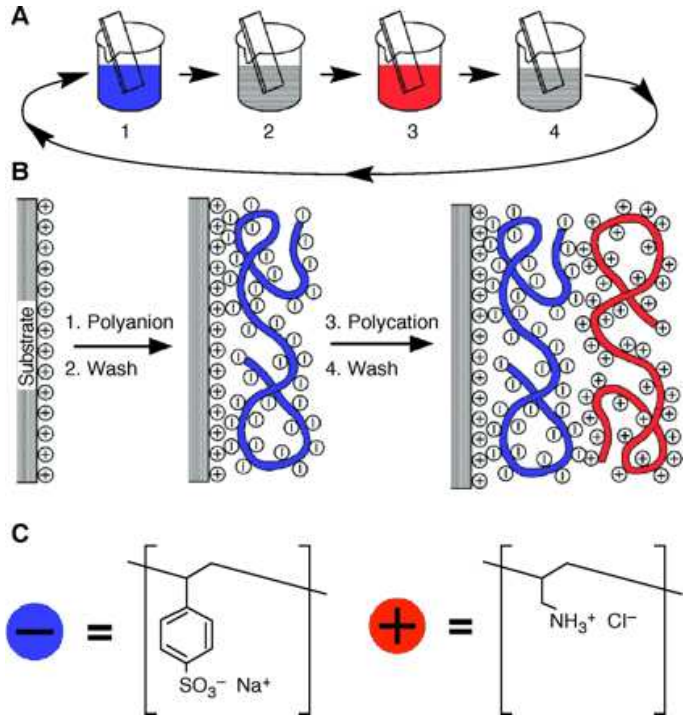

Figure 1: Layer-by-layer construction of polyelectrolyte films. *Steps 1 and 3* represent the adsorption of a polyanion and polycation, respectively, and *steps 2 and 4* are washing steps. The four steps are the basic build-up sequence for the simplest film architecture, $(A/B)_n$. The construction of more complex film architectures requires only additional beakers and a different deposition sequence. (B) Simplified molecular picture of the first two adsorption steps, depicting film deposition starting with a positively charged substrate. Counter ions are omitted for clarity. The polyion conformation and layer interpenetration are an idealization of the surface charge reversal with each adsorption step. (C) Chemical structures of two typical polyions, the sodium salt of poly(styrene sulfonate) and poly(allylamine hydrochloride). *Decher, G. Science 1997, 277, 1232-1237*

By deposition of a polycation and a polyanion layer-by-layer on a charged surface, polyelectrolyte films called polyelectrolyte multilayers can be constructed (**Figure 1**). This deposition process appears very versatile and allows the construction of films ranging in thickness from nanometers to microns. Since their discovery about 10 years ago [3], many different polyelectrolyte multilayers have been reported, with potential applications in fields as different as electro-optical devices [4], biomaterial coatings [5], or drug delivery [6].

The physicochemical properties of the multilayer architectures can be largely modified by varying the nature of the polyelectrolytes, the number of deposited layers, pH and ionic strength of the solutions [7,8]. For example, by changing the deposition conditions (pH or ionic strength), which strongly dictate the architecture of the films, it is possible to either prepare cytophilic or cytophobic film [9]. Also the cell behavior, in term of viability, adhesion, or cytoskeletal organization, may be dependent on the nature of the film constituents [9-14].

B16F1 melanoma cells (as a model system) have been demonstrated responding to small signal transduction molecules immobilized on the surface or being embedded into poly(glutamic acid)/ poly(L-lysine) (PGA/PLL) multilayer [15].

In general, polyelectrolyte films are constructed from a homo-polyanion and a homo-polycation solution. A way to change the properties of the multilayers could be the use of mixtures of different polyanions and/or polycations during the build-up. This goal can be approached in two ways: (i) any or both polyion solutions used for the construction of a polyelectrolyte film may contain a mixture of different polyanions or polycations. (ii) to let the ready polyelectrolyte film built up from homo-polyion solutions to interact with other polyions. The former possibility has been explored earlier [16]. In this thesis data related with the latter case are presented.

Polypeptide multilayers

A polypeptide multilayer film is defined as a multilayer film made of polypeptides. In certain cases, another type of polymer might be also involved in the fabrication process, for instance a chemically modified polypeptide [17], a non-biological organic polyelectrolyte [18], or a polysaccharide [19]. A polypeptide film might be used to provide specific bio-functionality on a surface that was otherwise bio-inert or to convert a bioactive surface into

one that is not adhesive to cells [18,20-22]. Study of polypeptide multilayer films involves at least two major and older fields: peptide structure and function, and polyelectrolyte multilayer films. The first being a significant area of basic research since the beginning, the second developed in the last decade of the 20th century.

Multilayer films of polypeptides are promising for the development of applications, aiming to achieve the following desirable features: biocompatibility, biodegradability, specific bio-molecular sensitivity, edibility, thermal responsiveness, and stickiness or non-stickiness.

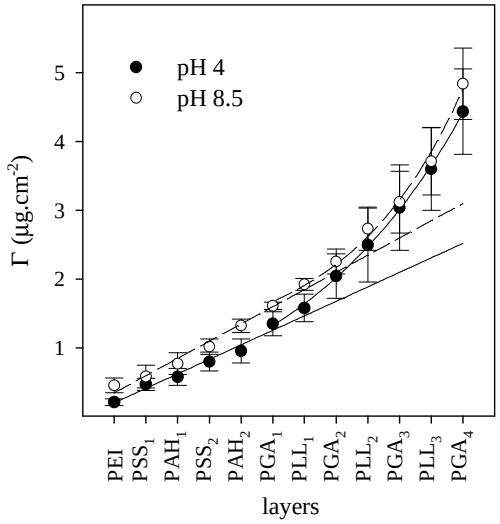

Figure 2: Typical layer-by-layer build-up of polyelectrolyte assemblies at pH 4 (•) and at pH 8.5 (o). The PEI, PSS, and PAH concentrations were 5 mg mL^{-1}; the PGA and PLL concentrations were 20 mg mL^{-1}. All polyelectrolytes were dissolved in 25 mM MES, 25 mM TRIS buffer containing 100 mM NaCl [16].

Polypeptides are ideally suited for such applications by virtue of their biochemical nature.

Depending on the components used, polyelectrolyte (among them polypeptide) films may exhibit linear or exponential growth regimes [16,23] (**Figure 2**). Exponential growth requires the free diffusion of at least one of the film components in the interior of the film [19]. Therefore these films have less ordered structures than the linearly growing films, which have been shown to exhibit some interpenetration between neighboring layers [3]. The polypeptide films made from poly(L-glutamic acid) (PGA) and poly(L-lysine) (PLL) used in the present study are of the exponential type [23].

1.2. Why Phospholipid bilayer on/in polyelectrolyte film?

Considering the extensively charged nature of the polyelectrolytes in these films, there is no chance for direct incorporation of non-polar, hydrophobic compounds into them. From the point of view of practical applications, however, it could be very useful if such compounds, e.g., different proteins, peptides, and drugs, could be incorporated.

For the incorporation of such protein molecules, at least lipid bilayers are needed. If once such bilayers were formed in the interior of polyelectrolyte films, they might be utilized as controllable internal barriers as well.

The present model membrane systems count mostly on the features of lipids. In the case of the liposomes the interaction with proteins is forced, with planar black lipid films and Langmuir-Blodget monolayers, only water soluble proteins can be studied. A lipid bilayer on the surface of a polyelectrolyte film could offer a real possibility for studying lipid-protein interactions in model membranes.

1.3. Why Fourier transform infrared spectroscopy?

Fourier transform infrared spectroscopy is based on an interferometer, where interferograms as a function of the position of a moving mirror are detected with a single detector. The infrared spectra are calculated via the inverse Fourier transformation of the detected interferograms. Due to its optical arrangement, large light intensities can be applied. The interferometer provides outstanding frequency reproducibility. As a consequence, FTIR spectroscopy offers a number of favorable features, which can be exceptionally useful in the case of biological studies [24-28].

Samples may be studied in a variety of physical states, like: solids, solutions, dispersions, oriented films; only small amounts of material are normally required. Whole infrared spectra (4000-400 cm^{-1}) can be recorded very quickly (in the range of seconds); it provides specific information about chemical bonding, molecular structures and dynamics from both the acyl chains and headgroups of the lipid molecules, and also provides information about the structure and dynamics of the protein components simultaneously in a single experiment.

FTIR spectroscopy can be applied even for such highly complicated systems as biological membranes, which represent delicate complexes of lipids and proteins. If the infrared spectrum of a biological membrane is recorded in D_2O-based medium the regions around 3050-2800 cm^{-1} and 1800-1400 cm^{-1} characteristic for lipid fatty acyl chains and protein secondary structure and dynamics, respectively, can be well seen. For illustration, the FTIR spectrum of a thylakoid membrane, prepared from a cyanobacterium (*Synechocystis*

PCC 6803) is shown in **Figure 3.** In the followings, a brief summary of the possibilities of infrared spectroscopy in the study of lipids and proteins is reviewed.

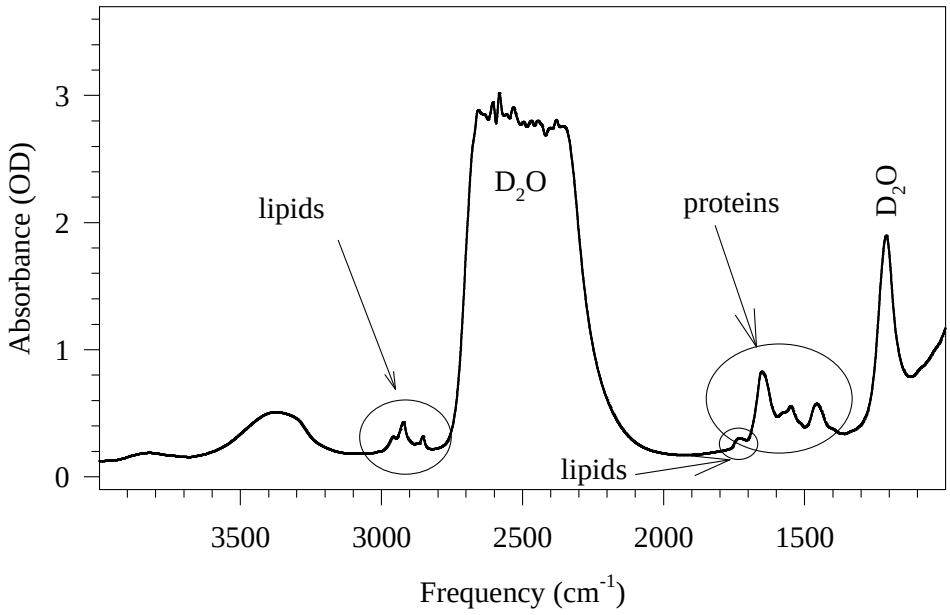

Figure 3: Infrared absorption spectrum of a thylakoid membrane.

1.3.1. FTIR study of lipids

Phospholipid head-group bands

The most characteristic vibrational bands of the head-group are those arising from the phosphate. Particularly, three bands appear in the 1300–1000 cm^{-1} region of a hydrated DPPC bilayer. As in the interfacial region, these bands are strongly dependent on the hydration state of the lipid and are sensitive to hydrogen bonding. The antisymmetric PO_2^- stretching mode appears around 1240 cm^{-1} in 'dry' phosphate and shifts to around 1220 cm^{-1} in fully hydrated DPPC. The symmetric PO_2^- stretching mode appears around 1086 cm^{-1} in hydrated dipalmitoylphosphatidylcholine (DPPC). A shoulder near 1060 cm^{-1} has been attributed to a R–O–P–O–R' stretching mode, which is equivalent to a P–O–C vibration with nonequivalent substituents [29]. In choline and ethanolamine glycerophospholipids, there are characteristic infrared bands due to these group vibrations, but they have no significant diagnostic value [24].

Acyl-chain vibrational modes

Bands arising from hydrophobic acyl residues have been assigned by comparing phospholipid bands to those of fatty acyl esters and other polymethylene chain compounds [30,31]. C–H stretching vibrations give rise to bands in the 3050–2800 cm^{-1} region. The asymmetric and symmetric CH_2 bands, around 2920 cm^{-1} and 2850 cm^{-1} (**Figure 4),** respectively, are the strongest ones in a phospholipid spectrum. These bands are

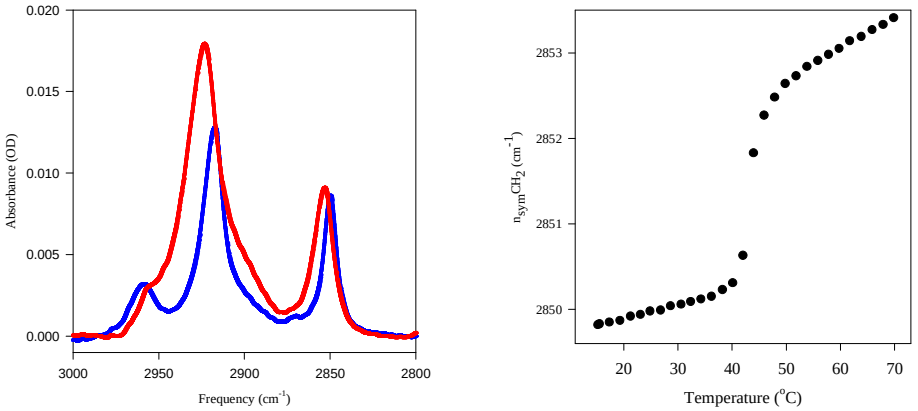

Figure 4: The frequency shift of the ν_{sym} CH_2 band of the FTIR spectrum of DPPC. The blue spectrum was recorded at 20 °C and the red at 70 °C.

also the most useful in the study of the physical properties of phospholipids. Vibrational bands corresponding to terminal methyl residues, CH_3, are found around 2956 cm^{-1} (asymmetric stretching) and 2870 cm^{-1} (symmetric stretching) appearing as shoulders of the stronger methylene bands.

Olefinic group bands, =C–H, arising from unsaturated hydrophobic chains are usually located around 3010 cm^{-1}.

Methylene bending bands (scissoring) are located around 1470 cm^{-1} and can split into two components in motion-restricted chains, and thus it can be used studying lipid domains in model membranes [26]. The CH_2 wagging progression is found between 1380 and 1180 cm^{-1} in the gel phase of saturated phospholipids as a series of shoulders on the phosphate band [31]. The methyl symmetric deformation mode around 1378 cm^{-1} that was assumed to be insensitive to changes in lipid morphology, was later found as sensitive to cochleate phase

formation in phosphatidylserine-containing model membranes [32]. Full or partial isotopic substitution of the acyl chains can be used to avoid interference with other components, i.e. in lipid mixtures or with proteins in lipid–protein interaction studies. In addition, selective deuteration can be used as an internal probe to study the characteristics of a specific methylene [33].

Phase transition

The methylene stretching vibrations are particularly useful in characterizing the gel-to-liquid crystalline phase transition and acyl chain conformations of lipid [24,34]. In practice, mostly the frequency of the CH_2 symmetric stretching band ($\nu_{sym}CH_2$) is monitored because it is relatively free from overlap by other vibrational modes. Its frequency has been shown to increase by 2-5 cm^{-1} at the gel to liquid-crystaline phase transitions temperature [35]. As it is shown in **Figure 4**, $\nu_{sym}CH_2$ increases from about 2850 cm^{-1} in the gel phase to about 2854 cm^{-1} in the liquid-crystalline phase of dipalmitoylphosphatidylcholine (DPPC) with a transition temperature (T_m) of 41.6 °C. The frequency up-shift is due to the increase of the ratio of the gauche/trans conformers in the acyl chains.

Table 1: Characteristic infrared absorption bands of lipids

Assignment	Approx. freq. (cm^{-1})
Olefinic – C-H stretch	3010
CH_3 antysimmetric stretch	2956
CH_2 antysimmetric stretch	2920
CH_3 symmetric stretch	2870
CH_2 symmetric stretch	2850
Ester C=O stretch	1730
$N^+(CH_3)_3$ antisymmetric bend	1485
CH_2 scissoring	1470
CH_3 antisymmetric bend	1460
$N^+(CH_3)_3$ symmetric bend	1405
CH_3 antisymmetric bend	1378
CH_2 wagging band progression	1400-1200
PO_2 antisymmetric strectch dry/hydrated	1240/1220
PO_2 symmetric stretch	1086
CH_2 rocking	730-720

The width of the band also increases due to the increased motional rates and to the larger number of conformational states of the hydrocarbon chains in the liquid-crystalline state. There are other conformation-sensitive vibrational modes of

the methylene and methyl groups in the region of 1500-700 cm^{-1} (**Table 1**). The CH_2 scissoring mode, for example, gives raise to bands around 1470 cm^{-1}; the number of these bands and their frequencies depend on acyl chain packing and conformation [36], but in the present work we have used only the frequency shift of the $\nu_{sym}CH_2$ band to characterize lipid fatty acyl chain disorder.

1.3.2. FTIR study of proteins

The IR spectrum of polypeptides and proteins contains several relatively strong absorption bands associated with the peptide bond, represented by CONH grouping. These bands are the amide bands (**Table 2**). These amide bands may reflect different aspects of the protein structure. For determining the secondary structure of a protein, the amide I band is most generally utilized; in the present work this band is used.

Table 2: The nine Amide bands of proteins

Amide bands	**Assignment**	**Approx. freq. (cm^{-1})**
Amide A	NH stretch	3300
Amide B	NH stretch	3100
Amide I	C=O stretch	1690-1600
Amide II	CN stretch, NH bend	1575-1480
Amide III	CN stretch,NH bend	1301-1229
Amide IV	OCN bend	767-625
Amide V	Out of plane NH bend	800-640
Amide VI	Out of plane C=O bend	606-537
Amide VII	Skeletal torsion	200

The amide I band (1690-1600 cm^{-1}) is by far the most studied because its line shape is sensitive to the type and amount of secondary structures and is not strongly influenced by the amino acid side chains [37]. The β-sheets have a strong absorption band near 1640–1630 cm^{-1} and a weaker band at high frequencies (>1680 cm^{-1}). β-sheets can be parallel or anti-parallel. If the amino terminal residue of each strand “points” in the same direction the sheet is considered parallel. Parallel β-sheets have a strong characteristic band around 1632 cm^{-1} and a weaker one around 1648 cm^{-1}. Anti-parallel sheets have characteristic bands around 1632 cm^{-1} (strong) and 1675 cm^{-1} (weak) [38]. The peaks for α-helices and random coils are located at 1660-1640 cm^{-1} and 1650-1640 cm^{-1}, respectively. The secondary structure sensitivity of amide I results from coupling between amide I oscillators that leads to vibrational states delocalized over large regions of the protein [39-41].

2. The Aim of the Work

Since biocompatible, bio-functionalized surfaces have increasing importance in nano-technological approaches of several biomedical applications, we wanted to reveal basic properties of such systems, which might strongly affect their later applications. For this goal we aimed to study:

- The build-up and the structure of polyelectrolyte films made from polypeptides (poly-(L-glutamic acid), PGA and poly(L-lysine), PLL),
- The interaction of PGA/PLL films with another poly amino acid, poly-(L-aspartic acid) (PAA), and with a protein (human serum albumin).

In view of the extensively charged nature of the polyelectrolytes in these films, there is no chance for direct incorporation of non-polar, hydrophobic compounds into them. Therefore, our goal was:

- To create a phospholipid bilayer, to form an internal barrier for the water-soluble compounds, and a potential carrier of hydrophobic proteins in a polyelectrolyte multilayer.
- Finally, we wanted to examine the behavior of our model membrane system in a biological environment by checking the effect of the lipid bilayer on the activity of bio-functionalized PGA/PLL films.

For these studies, we intended to use Fourier transform infrared (FTIR) spectroscopy to reveal the structure and molecular interactions, atomic force microscopy (AFM) to study the morphology of these films, and biological essays to follow the activity of the bio-functionalized surfaces.

3. Materials and methods

3.1. Sample preparations

The buffer: All experiments were performed in: tris(hydroxymethyl)aminomethane (Tris, 10 mM, Gibco BRL) and sodium chloride (NaCl, 0.15 M) pD 6.4 in deuterium oxide (99.9% D, Aldrich) buffer.

The polyanions: poly(L-glutamic acid) (PGA) (Sigma, P-4886, M_r = 17, 000 g·mol^{-1}) the concentration of solution 1 mg·mL^{-1}**,** and poly(L-aspartic acid) (PAA) (Sigma, M_r = 35, 400 g·mol^{-1}) in 1 mg·mL^{-1} solution.

Polycations: poly(ethyleneimine) (PEI, Aldrich, M_r = 750,.000 g·mol^{-1}) in 5 mg·mL^{-1} solution and poly(L-lyisine) (PLL, Sigma, M_r = 32, 600 g·mol^{-1}) in 1 mg·mL^{-1} solution.

Proteins: The concentration of the Human serum albumin (HSA) (bought in lyophilised form from Sigma) solutions was Sigma was 1 mg·mL^{-1}.

Lipids: 2 mg of dipalmitoylphosphatidylcholine (DPPC) was dissolved in 200 µL chloroform:methanol (2:1) in an appropriate test tube. Afterward the solvent was evaporated by N_2 flow. Then 8 mL of Tris buffer was added to the dried DPPC, and liposomes were formed by sonication. Sonication was applied in several steps until turbidity was observed in the test tube. No special care was taken to have unilamellar liposomes.

Peptide: Gramicidin A (GRA) (Fluka, M_r = 1,884 g·mol^{-1}) was dissolved together with DPPC at a 1:10 molar ratio in 2,2,2-trifluoroethanol (TFE). After 2 h of incubation at room temperature, the sample was dried first with N_2 and then under vacuum overnight. Afterwards, all treatments were the same as those described above for pure DPPC.

Cell culture: Murine B16F1 cells, a metastatic subline of murine B16 melanoma were a gift from Dr S. Brézillon (CNRS UMR 6198, Reims, France). They were cultured at 37 °C in 5% CO_2 in the presence of 100 IU/mL penicillin-streptomycin (Gibco, France). The RPMI-1640 growth medium (Gibco) was supplemented with 10% foetal calf serum (Gibco, France). Cells were passed every 3rd day at a ratio of 1:20 upon reaching confluence.

3.2. Measurement of melanin production

For counting, the cells were dissociated from the surface as follows: The growth medium was removed (and later used for melanin determination), the cells were rinsed with PBS (Phosphate Buffered Saline, 0.01 M phosphate buffer, 0.137 M sodium chloride) (400 µL/well), then 200 µL trypsin/EDTA (0.5%) (Gibco, France) was added for 5 min, at 37 °C, afterwards 200 µL fresh growth medium was added and the cells were collected. Counting was done under microscope using a hemacytometer with Neubauer ruling.

Melanin determination: The firstly removed growth medium (at the 2,3,4,5th days of the culturing) and all the other solutions used for preparing the cells for counting and the cells themselves were put together and centrifuged down (5 min, 4500 RPM, Sigma 1-14 Eppendorf centrifuge) For opening the cells, the pellet was re-suspended in 500 µL of 0.85M potassium hydroxide and 10% dimethyl sulfoxide, at 80 °C for 90 min. Afterwards 100 µL equivalents were put into the wells of an ELIZA plate and the absorption was measured at 405 nm (indicating melanin content) [15] in a micro plate reader. Each biological experiment was performed with three parallel manipulations. The presented data are the average of these triplicates.

3.3. Construction of Polyelectrolyte Multilayers

Multilayer polyelectrolyte films were built by the layer-by-layer (LBL) consecutive adsorption method [3] (**Figure 1**). In our case the polyelectrolytes were brought into contact with the solid support, a ZnSe internal reflection element, by being circulated with a peristaltic pump above the crystal (**Figure 5**). The build-up of the polyelectrolyte film

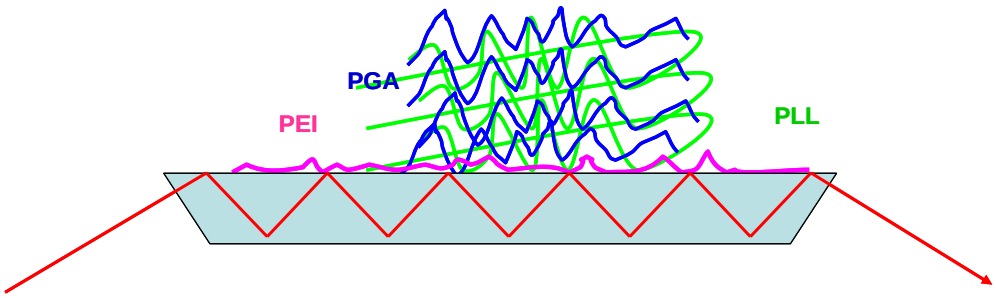

Figure 5: Model of polyelectrolyte multilayer on the surface of Attenuated Total Reflection (ATR) crystal made from ZnSe.

started with circulating PEI for 10 min in the form of a 5 mg·mL^{-1} solution. (Rinsing with pure buffer for 10 min followed all the adsorption steps.)

In the next step PGA or PAA was allowed to adsorb from 1 mg·mL^{-1} solutions. After another rinsing, for the same period of time, the polycation solution containing 1 mg·mL^{-1} of PLL was circulated above the film surface. This procedure was repeated until the: **PEI-(PGA/PLL)$_6$** or **PEI-(PAA/PLL)$_6$** architectures were achieved.

For the PGA-PAA and PAA-PGA competition studies, the construction of the film was stopped at the stage of PEI-(PGA/PLL)$_5$-PGA, then PAA was allowed to interact with the film. After the film structure came into a steady state, the last PLL layer was added. Thus, the final architecture was: **PEI-(PGA/PLL)$_5$-PGA + PAA-PLL**. The same procedure was used for the **PEI-(PAA/PLL)$_5$-PAA+PGA-PLL** films. The steady state was declared when there were no more changes in the infrared spectra recorded from the film. In general, we allowed the film to reach equilibrium by waiting overnight.

The films for the biological essay were built on 14 mm diameter glass slides (CML, France). These glass slides first were cleaned with ethanol and were let for 30 min in 2% Hellmanex at 100 °C and extensively rinsed with Milli-Q water, then let for 10 min in 1M HCl solutions at 100 °C and extensively rinsed again with Milli-Q water and were placed into culture plates (24-well plates, NUNC, France)

For the biological tests, we have used standard and bio-functionalized PGA in the PGA/PLL multilayer. The bio-functionalized PGA contained covalently bound α-MSH. α-MSH is a small peptide hormone (*Ac-Ser-Tyr-Ser-Met-Glu-His-Phe-Arg-Trp-Gly-Lys-Pro-Val-NH$_2$)* named melanocyte stimulating hormone or α-melanocortin. It is known to interact with the cytoplasmic-membranes of the cells and triggering melanin production [42].

The following architectures were built up on these glass slides:

(1) (PLL/PGA)$_5$/PLL;

(2) (PLL/PGA)$_5$/PLL/PGA-α-MSH;

(3) (PLL/PGA)$_5$/PLL/PGA-α-MSH/DPPC

Once these films were created on the glass slides, the slides were put into the well, and sterilised with UV irradiation for 15 min. Then about 50.000 cells in 0.5 mL medium were added and culturing started.

3.4. Protein adsorption

HSA (Sigma) was dissolved in the same buffer as the polyelectrolytes and was circulated above the polyelectrolyte film at a concentration of 1 $mg \cdot mL^{-1}$ for at least 20 min. The progress of the adsorption was first followed by rapidly recorded low signal-to-noise ratio infrared spectra. After the saturation of the adsorption, the protein excess was washed down from the polyelectrolyte film surface with pure buffer. Only then were high signal-to-noise ratio infrared spectra recorded and considered as those of the adsorbed proteins.

3.5. Phospholipid Bilayer on the Surface of the multilayer polyelectrolyte film

For being adsorbed, the DPPC liposome solution was circulated first at 25 °C above the $(PGA\text{-}PLL)_5$-PGA film. During this period, only a very small lipid signal could be observed in the 3000-2800 cm^{-1} region of the infrared spectrum, as monitored continuously during the adsorption procedure. Then, the temperature was increase to 45 °C, i.e. above the phase-transition temperature of DPPC (41.6 °C), and the liposomes remained circulating overnight. Then the temperature was decreased to ambient. This heating-cooling cycle resulted in a large increase (up to ten-fold) of the lipid signal. Then, the cell was washed with pure buffer. Washing did not affect the amount of the adsorbed DPPC considerably. The intensity of the lipid infrared spectrum remained fairly constant afterward, and the lipid bilayer on the top of the polyelectrolyte film could survive as many phase-transition measurements as wanted.

In the case of incorporation of a peptide into the lipid bilayer, the procedure was the same as for the pure DPPC.

3.6. Infrared Spectroscopy

Fourier transform infrared (FTIR) spectra were recorded on a Bruker IFS66 FTIR spectrometer in attenuated total reflection (ATR) mode using trapezoidal or cylindrical (Circle Cell®) ZnSe crystals as internal reflection elements. Single-beam spectra were recorded at each stage of the polyelectrolyte film construction and the protein adsorption. For each spectrum, 1024 or 2048 scans were collected (at 2 cm^{-1} spectral resolution) with a liquid nitrogen-cooled mercury cadmium telluride (MCT) detector.

Spectrum manipulations and evaluations were done with the SPSERV© software, developed by Dr. Cs. Bagyinka (Institute of Biophysics, Biological Research Centre, Szeged, Hungary).

3.6.1. Singular Value Decomposition analysis of the infrared spectra

For analyzing the dynamics and phase properties of the adsorbed/embedded DPPC bilayer in polyelectrolyte multilayer film, we used the singular value decomposition (SVD).

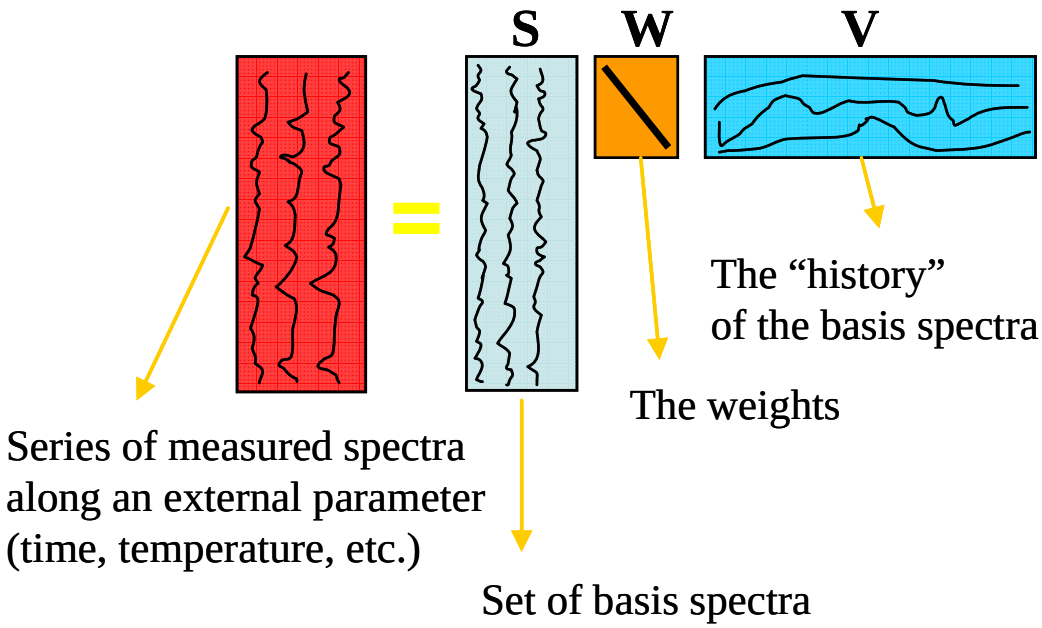

Figure 6: Singular Value Decomposition (**SVD**) analysis is a reduced representation of the data matrix in terms of a set of basis spectra (**S**), an associated set of temperature-dependent (or other variable dependent) amplitude vectors (**V**) and a diagonal matrix with the weights of the species (**W**).

SVD was applied as described in details by Henry and Hofrichter [43], and citations therein. Briefly, if a system as a function of an external parameter (temperature, concentration, time, etc.) contains $\mathbf{s_i}$ species (**Figure 6**), which are spectrally distinguishable, at any moment the measured spectrum can be described as a linear combination of the spectra of these $\mathbf{s_i}$ species. The output of the SVD analysis is a reduced representation of the data matrix in term of a set of basis spectra, an associated set of temperature- (or other variable) dependent amplitude

vectors ($\mathbf{v_i}$), and a diagonal matrix with the weights of the $\mathbf{s_i}$ species ($\mathbf{w_i}$). Since the set of output components is ordered by decreasing size, each subset consisting the first **j**-components provides the best **j**-component approximation of the data matrix. Thus, a set of $\mathbf{s_j}$ output components can be selected, which describe the data matrix within experimental precision.

When spectra taken as a function of the temperature are to be analyzed, the $\mathbf{s_1}$ basis spectrum shows a temperature average, $\mathbf{s_2}$ shows the largest changes, which have to be combined with the $\mathbf{s_1}$ spectrum to get the actual spectrum at a given temperature. The $\mathbf{v_2}$ amplitude vector gives the temperature dependence of the largest change, manifested in the $\mathbf{s_2}$ spectrum.

3.7. Atomic Force Microscopy (AFM)

For the AFM measurements, as supports, freshly cleaved mica (SPI-Chem Mica Sheets, Structure Probe, Inc., West Chester, PA) surfaces were used. This surface is ideal for AFM measurements since it is free from any contamination and flat at atomic level.

On the mica surface, the same PEI-$(PGA\text{-}PLL)_5$-PGA films were constructed as for the FTIR experiments. When needed, the DPPC bilayer was also formed the same way on the surface of the polyelectrolyte film as described above for the FTIR measurements. AFM measurements were carried out with an Asylum MFP-3D head and Molecular Force Probe 3D controller (Asylum Research, Santa Barbara, CA). The driver program MFP-3D Xop was written in IGOR Pro software (version 5.04b, Wavemetrics, Lake Oswego, OR). Silicon nitride cantilevers (Bio-Lever BL-RC150VB-C1, Olympus Optical Co., Ltd., Tokyo, Japan) were used for the experiments. The calibration of the spring constant of each cantilever was performed individually by thermal fluctuation technique [44-46]. Measurements were made both in alternative contact (AC) and in contact modes in buffer. Typically 512 x 512 point scans were taken at 1 Hz scan rate.

In AC mode, the cantilever is oscillated usually at or near its resonance frequency, with a few nanometer amplitude and its damping caused by the sample surface is kept constant. Any surface roughness causes variations on the amplitude value, which is used to drive the feedback. Any deviations from the set point amplitude value of the oscillating cantilever are recorded and the error signal image constructed. The AC mode operation was introduced to

minimize tip-sample interaction time during scanning and it is suitable for investigate soft biological materials by reducing the possible sample damages caused by the relatively hard tip.

In contact mode, the cantilever's bending (deflection) is kept constant at a certain, predefined set point and for any deviation from this value, caused by the surface roughness, the vertical piezo reacts. By this predefined set point the force exerted by the cantilever on the sample can be kept constant and determined by knowing the parameters of the cantilever [47]. Error signal (deflection) images are captured recording any deviation from the set point deflection value of the cantilever during scanning.

4. Results and Discussion

4.1. Modelling the structures of PGA-PLL, PAA-PLL films

Before starting analysing the structure of polyelectrolyte films, we have tried modelling the structure of amino acids, which were used in this work. Fascinating is, that the small structural difference between the anions when they interact with the same cation, causes very different film structures. The structures of the three amino acids used in the experiments are shown in **Picture 1**.

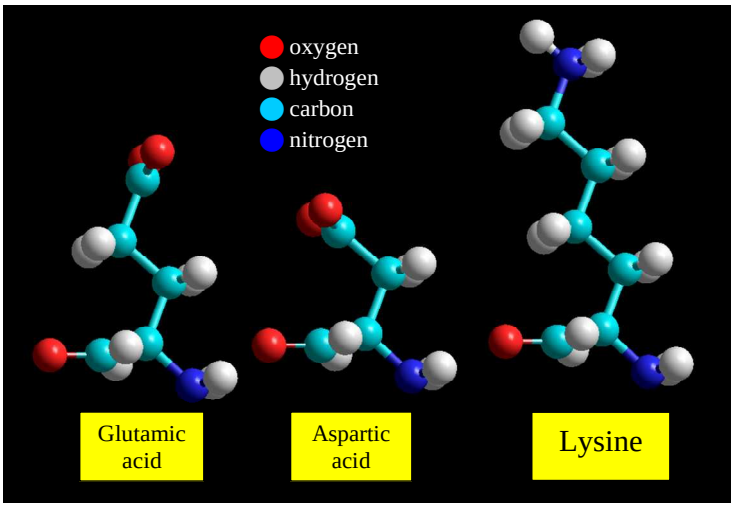

Picture 1: Structures of the amino acids involved in the present work

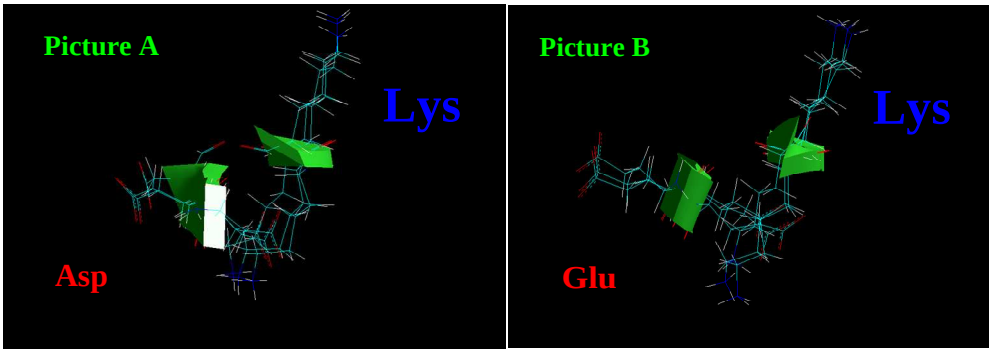

Picture 2: A - a cross section of a PAA/PLL; **B** - PGA/PLL from the same projection

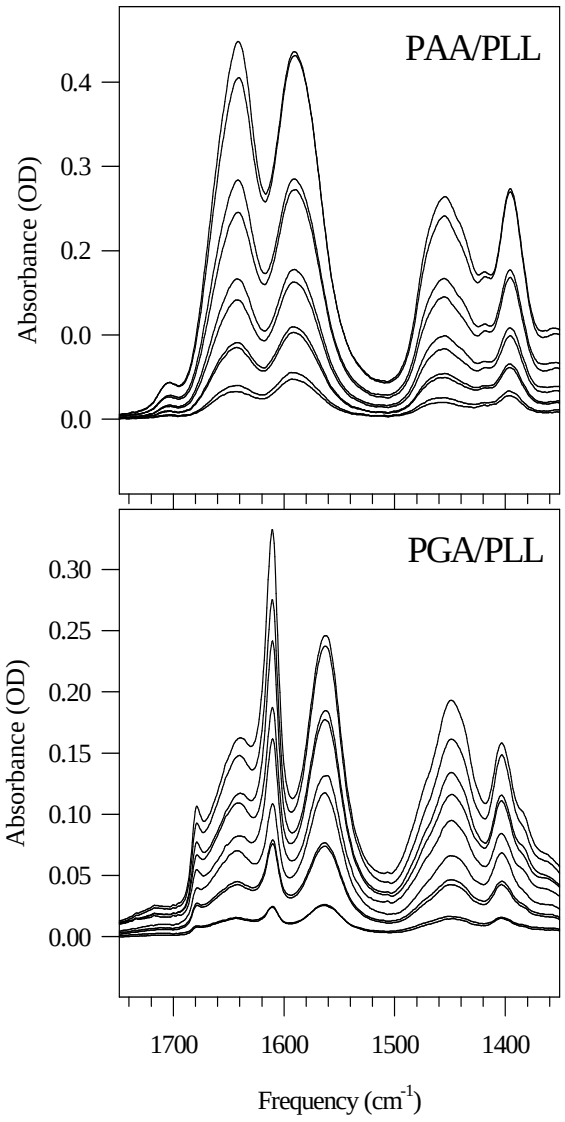

Figure 7: Infrared spectra of the growing polyelectrolyte films. Odd spectra are PAA or PGA, respectively; even spectra show the film structure after the adsorption of the complexing PLL. Note the difference in the Amide I region, PAA/PLL films are dominated by a broad band around 1637 cm^{-1}, indicating some α-helical, some random, and some β-structures. PGA/PLL films have two narrow bands around 1611 and 1685 cm^{-1}, indicating a strong intermolecular β-structure between PGA and PLL.

A cross-section of a PAA/PLL 'chain is given in **Picture 2A**. It can be seen, that, indeed, from such chains multilayered structures can be built, since there are well-separated positively and negatively charged 'edges' of the chain. In **Picture 2B**, PGA/PLL is shown from the same projection. Due to the shorter side chain in aspartic acid, the structure of the PAA/PLL film is more dens than that of the PGA/PLL film (**Picture 2B**). (Imagine piling up the structure in **Picture 2A**, by rotating each second layer by 180^{o}.)

The changes in the infrared spectra of pure PAA/PLL and PGA/PLL films upon their layer-by-layer construction it is shown in **Figure 7**. With increasing number of layers the "ordering" effect of PLL is also increasing (2^{nd}, 4^{th}, 6^{th}, 8^{th}, 10^{th} spectra from the bottom).

By ordering, that those features, which are related to the characteristic secondary structure of the given film, increase faster than the other polyelectrolyte-related bands. The increase of the band at around 1638 cm^{-1} in PAA/PLL is faster than the increase of the PAA COO^{-} band at 1594 cm^{-1}, the increase of the 1610 cm^{-1} band in the PGA/PLL film is faster than that of the 1567 cm^{-1} PGA

COO^- band. Such growth characteristic is the consequence of the exponential growth of the films. Exponential growth means that the amount of the incorporated material is an exponential function of the number of the layers in the film (as it is illustrated in **Figure 2**). It can be interpreted that at least one of the components can more or less freely diffuse in the film. Thus, the new molecules coming into the film upon the construction of the forthcoming layers can find their way into the interior of the already existing film, and improve the film structure. Therefore the structure-related infrared bands are increasing also faster than linear with the number of the layers.

4.2. The structure of the PGA-PLL and PAA-PLL films studied by FTIR spectroscopy

First, PEI-$(PGA\text{-}PLL)_6$ films were constructed. The infrared absorption spectrum of the $(PGA\text{-}PLL)_6$ film is given in **Figure 8A**. This film has a definite secondary structure, dominated by extended β-sheets as indicated by the strong, narrow band at around 1610 cm^{-1} and by the accompanying weaker band at around 1679 cm^{-1}. This β-structure is formed due to the interaction between PGA and PLL as they are built into the film architecture [48]. Such a β-structure can be observed generally upon heat-denaturing of proteins, when large, 'intermolecular' β-sheets are formed in the aggregates [49,50]. In the PGA-PLL films there is a broad band centered at around 1638 cm^{-1}. The asymmetric COO^- group vibration of PGA give a strong contribution at around 1567 cm^{-1}, and there is a weak, broad band due to the COOH groups, which can be resolved into two components in the fourth derivate spectrum (1707 and 1724 cm^{-1}).

The situation is markedly different when $(PAA\text{-}PLL)_6$ films are constructed (**Figure 8B**). The amide I region is dominated by a strong band at around 1637 cm^{-1}. In PAA the asymmetric vibration of the COO^- groups is at around 1594 cm^{-1}. The COOH vibrations of PAA are also visible in the form of a rather weak band at around 1705/1733 cm^{-1}. The assignment of the band at 1638-1637 cm^{-1}, which is present both in the PGA/PLL and the PAA/PLL spectra, albeit at very different extent, is not equivocal. In pure PLL, a band at around 1635 cm^{-1} was assigned to α-helices; in pure PGA and PAA, somewhat higher frequencies were reported also for α-helices [49,51]. In proteins, this frequency is characteristic of the low frequency component of the extended chains i.e. β-structures [38].

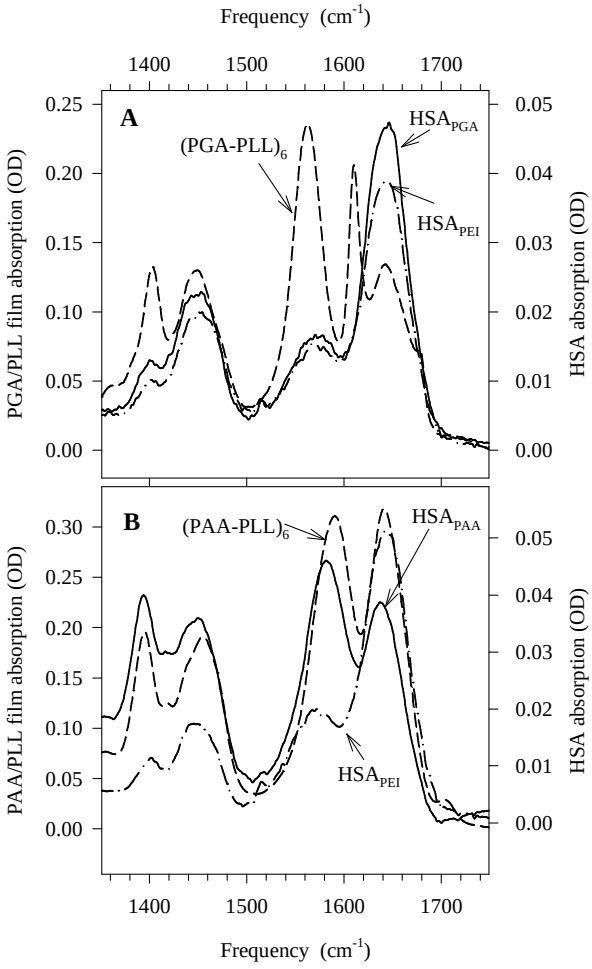

Figure 8: FTIR-ATR spectra of $(PGA\text{-}PLL)_6$ (panel A) and $(PAA\text{-}PLL)_6$ (panel B) polyelectrolyte films. HSA_{PGA}, HSA_{PAA}, and HSA_{PEI} are the FTIR-ATR spectra of human serum albumin adsorbed onto the surface of $(PGA\text{-}PLL)_6$, $(PAA\text{-}PLL)_6$ and a single PEI layer, respectively.

We know that the observed spectra of the PGA/PLL and PAA/PLL are formed upon the complex formation [52]. Due to the increased heterogeneity of the amino acids in the complexes as compared to the homo-polymers, we would lean toward the β-sheet interpretation. This possibility is also supported by the presence of a surely α-helix related component in PAA at 1656 cm^{-1} (PAA_{PEI} in **Table 3**). This point would need further investigation, but for the moment it does not interfere with our topic of interest. Whatever the precise assignments of the component bands in the amide I region are it is evident that the secondary structures of the PGA/PLL and PAA/PLL films are markedly different.

4.2.1. The effect of the polyelectrolyte film structure on the structure of the adsorbed human serum albumin (HSA)

For being adsorbed, human serum albumin (HSA) (1 $mg.mL^{-1}$) has been circulated above the PEI-$(PGA\text{-}PLL)_6$ film, followed by washing with pure buffer. The infrared absorption spectrum of the adsorbed HSA is shown in **Figure 8A** (HSA_{PGA}). As a kind of reference, the infrared absorption spectrum of HSA adsorbed onto a single layer of PEI is also given (HSA_{PEI}). As it can be seen from the identical shapes of the amide I bands of HSA_{PGA}

and HSA_{PEI}, HSA does not suffer considerable structural changes upon being adsorbed onto the surface of the $(PGA\text{-}PLL)_6$ film. The amount of the adsorbed protein is high (≈ 50 mOD) as compared with the adsorption of other proteins onto different polyelectrolyte films (≈ 8 mOD) [53,54].

Table 3.: Infrared bands of $(PGA/PLL)_6$, $(PAA/PLL)_6$ polyelectrolyte films, and of human serum albumin adsorbed onto these films (HSA_{PGA}, HSA_{PAA}), and of HSA adsorbed onto a single layer of PEI (HSA_{PEI})[a].

PGA/PLL	HSA_{PGA}	PAA/PLL	HSA_{PAA}	HSA_{PEI}	assignment
4th derivate*	4th derivate*	4th derivate*	4th derivate*	4th derivate*	
	1514		1515	1514	tyrosine
	1538		1540	1532	amide II'
	1557			1548	amide II'
1567		1573	1568	1566	COO^-
1581	1583		1584	1584	COO^-
1595		**1594**			COO^-
	1601			1606	
1610					β-structure
1624	1628		1629	1628	β-structure
1638[c]		**1637**[c]			β-structure[c]
					unordered
	1652		1653	1653	α-helix
1665		1664			
1679	1678		1676	1676	β-structure
1693				1693	
1707	1702	1705	1707	1710	COOH
1724	1731	1733	1727	1727	COOH

[a]Bold-faced numbers indicate the frequencies of the maxima in the PGA/PLL and PAA/PLL spectra.
[*]Component band frequencies were obtained by fitting Lorentzian curves around the maxima of the fourth derivates of the original infrared absorption spectra shown in **Figure 8.** This was possible, because, before taking derivates, the original spectra were Fourier smoothed as described later**.**
[c]The assignment of this band might be different for proteins and for poly-(amino acids).

When HSA was adsorbed onto the surface of a $(PAA\text{-}PLL)_6$ film, a quite different absorption spectrum was obtained (HSA_{PAA} in **Figure 8B**). At a first glance, this PAA-related HSA_{PAA} spectrum looks very similar to the infrared spectrum of PAA. But there are

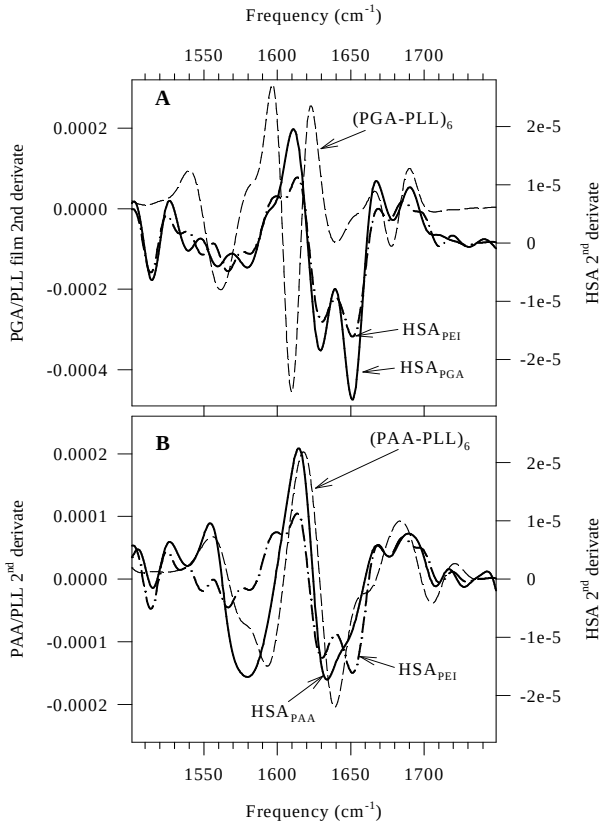

Figure 9: Second derivates of the FTIR-ATR spectra (shown in **Figure 8**) of HSA_{PGA}, HSA_{PAA}, HSA_{PEI}, $(PGA\text{-}PLL)_6$, and $(PAA\text{-}PLL)_6$. The second derivates were obtained after subtracting water vapor and Fourier smoothing as described later. Note, that HSA_{PGA} and HSA_{PEI} are very similar (panel A), and HSA_{PAA} is different from them (panel B).

differences as well, which indicate the protein contribution to this infrared spectrum:

(i) The HSA_{PAA} spectrum does not contain the characteristic COOH band at around 1705 cm^{-1}. (ii) Unlike $(PAA\text{-}PLL)_6$, which has a single component at 1637 cm^{-1}, the dominating band in the middle of the amide I region of HSA_{PAA} contains two components, at 1629 cm^{-1} and 1653 cm^{-1}, corresponding to β-structure and α-helices, respectively (see **Table 3**.). (iii) The major COO^- component in HSA is at 1584 cm^{-1}, while in $(PAA\text{-}PLL)_6$, this band is at 1594 cm^{-1}. Since there are major underlying secondary structures in the polyelectrolyte films, the absolute determination of the secondary structure of the adsorbed protein might be ambiguous. Therefore, we limited our goals to the determination of the presence or absence of certain bands in the different cases.

The structural similarities and differences can be better visualized when taking the second derivates of the original absorption spectra. This is presented in **Figure 9**. Here, minimums show the component band frequencies. Note that the structure of HSA is practically the same whether it is adsorbed onto a $(PGA\text{-}PLL)_6$ film, or onto a single layer of PEI (HSA_{PGA} and HSA_{PEI} in **Figure 9A**). This is not the case when HSA is adsorbed onto a $(PAA\text{-}PLL)_6$ film (HSA_{PAA} in **Figure 9B**). HSA_{PAA} has a component band at 1629 cm^{-1}, and a non-resolved shoulder at 1653 cm^{-1} (**Table 3**), and there are large differences between HSA_{PAA} and HSA_{PEI} in the other parts of the infrared spectrum as well. (It should be

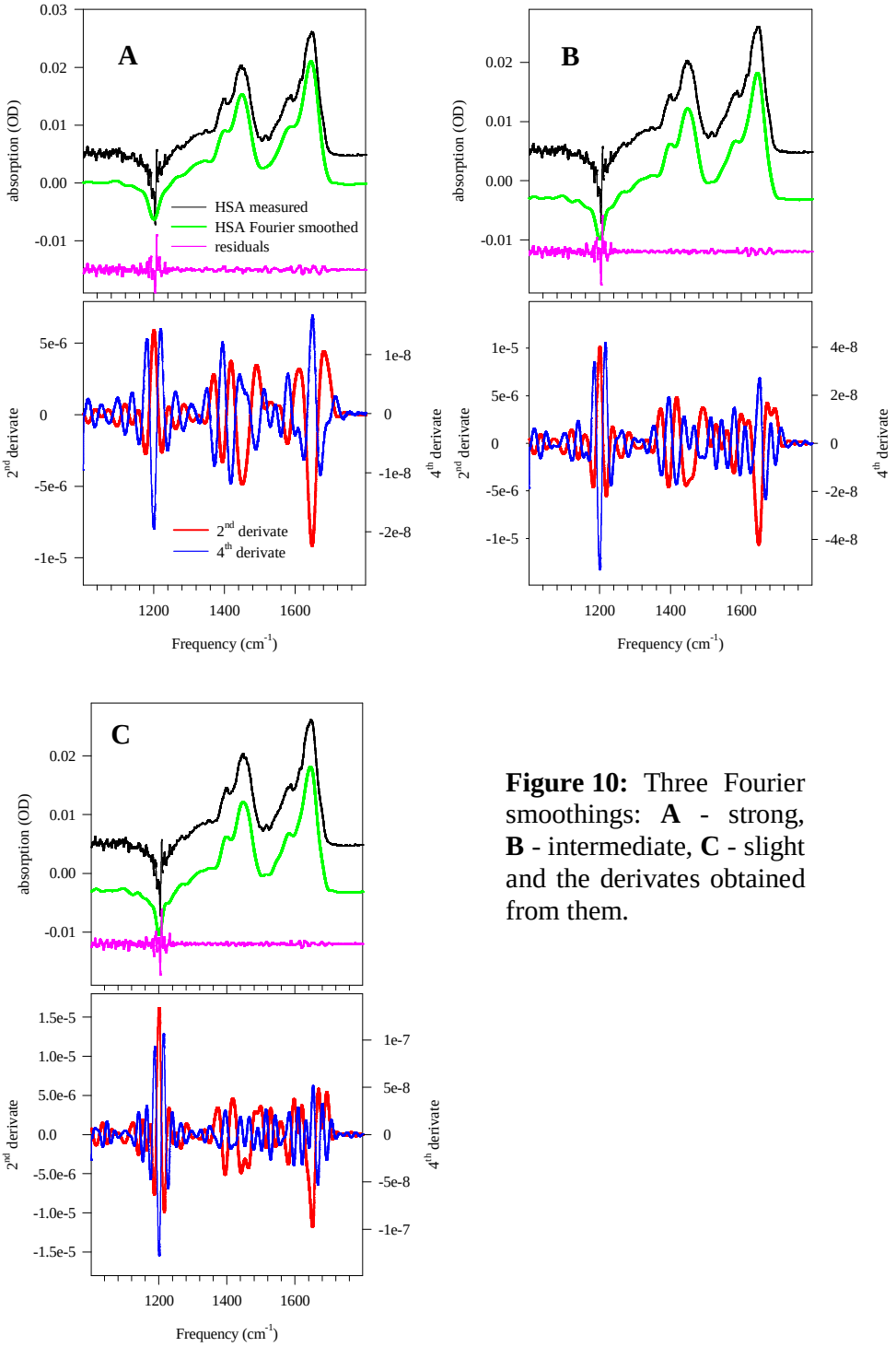

Figure 10: Three Fourier smoothings: **A** - strong, **B** - intermediate, **C** - slight and the derivates obtained from them.

mentioned here, that when we speak of features of the HSA_{PAA} spectrum only, it is a simplification. Those features do not necessarily originate from the protein alone they might

be the result of changes in the polyelectrolyte film due to the protein-polyelectrolyte interaction with the protein as well, but we cannot separate the changes according to their origins. The difference spectrum registers the net result of all changes.)

Looking at the maximums of the fourth derivates of the infrared absorption spectra one can further increase the frequency resolution of the component bands. Since the noise is dramatically increasing with the order of the derivate, in most cases the use of the fourth derivate to predict component bands is illusory when it is calculated directly from the original spectrum, even if polynomial smoothing is applied. By Fourier smoothing as suggested by Schwinte et al. [53], the noise could be in such extent eliminated without causing considerable distortion in the spectrum that the fourth derivates became appropriate for component band frequency determination.

To prove the credibility of Fourier smoothing and the following determination of component band frequencies from the second and the fourth derivates, we show three examples in **Figure 10** a strong, an intermediate, and slight Fourier smoothing and the derivates obtained from them.

The residuals between the measured and the Fourier-smoothed spectra do not show any major distortion as evidenced by the straight baseline of the residuals. The decreasing smoothing has an effect on the features in the amide I region of the residuals. With decreasing smoothing, these features, which might be related to secondary structure elements, become less and less structured. The noise of the fourth derivate even in the case of slightest smoothing remains at an acceptable level. To judge this, regard the protein-free 1800-1700 cm^{-1} region.

It can be seen, that with decreasing smoothing, the derivates become more and more structured. Components, which were not resolved at strong smoothing or were indicated only by a shoulder, can be nicely distinguished.

A detailed analysis of the component bands for all infrared spectra determined from the fourth derivates of the infrared absorption spectra is given in **Table 3**. Only the frequencies of the component bands are given, they indicate the presence of the component bands, but tell nothing about their relative intensities.

4.3. Competition between PGA and PAA

Since glutamic and aspartic acids are chemically very similar (**Picture 1**) (the only difference is that glutamic acid has two, whereas aspartic acid has only one CH_2 groups in his side-chain), it is an interesting problem, whether they can replace each other in their differently structured films. There are chances for this since according to Optical Waveguide Lightmode Spectroscopy (OWLS), the layer-by-layer growth of the PGA/PLL film follows exponential pattern [23]. This means that at least one of the polyelectrolytes can freely diffuse in the interior of the film. Therefore, in these films, there should be room for post-construction modifications like the interaction with a second polyanion.

This is a completely new situation as compared with the one studied earlier [55]. There, mixed $[(PAA+PGA)\text{-}PLL]_n$ films were constructed from co-solutions of PGA and PAA, thus, there was a possibility for 'free choice' when a molecule had to be selected for the film under construction. Here, the $(PGA\text{-}PLL)_n$ or $(PAA/PLL)_n$ films are ready and have their characteristic secondary structures when they are brought into contact with the other polyanion. This experiment raises the following questions: (i) how definite and stable are the initial structures, (ii) are there chances for exchanging one polyanion for the other, (iii) and if so, what are the structural consequences?

Therefore, $(PGA\text{-}PLL)_5$-PGA (or $(PAA\text{-}PLL)_5$-PAA) films were let to interact with PAA (or PGA). Thus, first a transient architecture $(PGA\text{-}PLL)_5$-*PGA+PAA* (or $(PAA\text{-}PLL)_5$-*PAA+PGA*) was obtained. The interaction with the second polyanion induced certain exchange between the two polyanions. In the after-addition minus before-addition of the second polyanion difference spectrum, the contribution of the secondly added polyanion was always positive, the contribution of the primary polyanion was always negative. These difference spectra are shown in **Figure 11**. The infrared difference spectra induced by the interaction of PAA with a PEI-$(PGA/PLL)_5$-PGA film (PAA_{PGA} spectrum in **Figure 11A**), and that of PGA with a PEI-$(PAA/PLL)_5$-PAA film (PGA_{PAA} spectrum in **Figure 11B**). These difference spectra (open symbols) were evaluated by the following logic: The difference spectra observed due to entering and leaving polyanions is the net result of the exchange. In the film, PGA and PAA form complexes with PLL. For leaving PGA or PAA, such a complex has to brake up; for an incorporating PAA or PGA, such a complex has to be formed.

We know that the infrared spectra of PGA, or PAA are different from that of the (PGA/PLL), or (PAA/PLL) complexes.

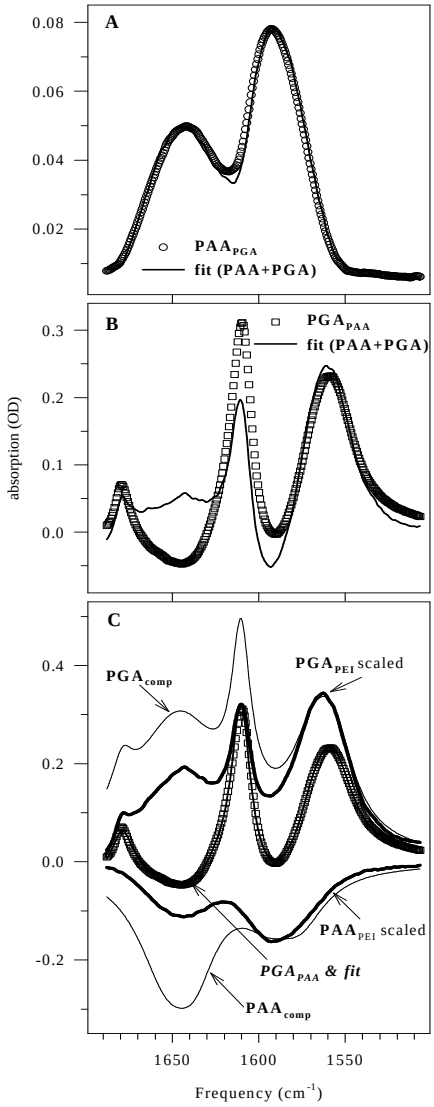

Figure 11: Difference FTIR-ATR spectrum due to adding of PAA to a PEI-$(PGA/PLL)_5$-PGA film (PAA_{PGA}, panel A); adding of PGA to PEI-$(PAA/PLL)_5$-PAA film (PGA_{PAA}, panel B). Open symbols indicate measured spectra, the solid line is the result of a fit obtained by the linear combination of pure PAA and PGA spectra adsorbed onto a PEI single layer (PAA_{PEI}, and PGA_{PEI}), respectively. PAA_{PEI} and PGA_{PEI} are shown with scaled amplitudes as obtained for PGA_{PAA} (panel C). PGA_{comp} and PAA_{comp} are calculated spectra obtained by summing up all PGA- and PAA-related components, respectively, used in the multi-component fit of PGA_{PAA} (the result of the multicomponent fit is the solid line within the open symbols, panel C). The components used in the multicomponent fit are listed in **Table 3**. For details, see the text.

Therefore, we have tried to fit these difference spectra with the linear combination of pure PAA and PGA spectra. The spectra of the first PAA and PGA layers on PEI (PAA_{PEI} and PGA_{PEI}, shown in **Figure 11B**) were used for this purpose. The good fit obtained for PAA_{PGA} (**Figure 11A**) by using the linear combination of PAA_{PEI} and PGA_{PEI} indicates that neither PAA nor PGA was suffering structural changes upon the PGA→PAA exchange. A rough estimation, based on the normalized amide I band intensities of the PGA_{PEI} and PAA_{PEI}

spectra used for the fit gave for one leaving glutamic acid unit seven incorporating aspartic acid units during the exchange. (This estimation includes the approximation that the extinction coefficients of PGA and PAA in the amide I region are the same.)

In contrast to PAA_{PGA} spectrum, when the PGA_{PAA} spectrum was fitted with the linear combination of the same PAA_{PEI} and PGA_{PEI} spectra, large differences remained between the measured and fitted spectrum, especially in the amide I region (**Figure 11B**). The same rough estimation as the one used above gave three leaving aspartic and four incorporating glutamic units for this poor fit. The spectra of PAA_{PEI} and PGA_{PEI} used in this fit (and also for fitting PAA_{PGA} above) are shown in **Figure 11C** ($PAA_{PEI\text{-}scaled}$ and $PGA_{PEI\text{-}scaled}$). Their intensities, however, are scaled, as required by the fit of PGA_{PAA} in **Figure 11B**. The discrepancy between the measured and the fitted spectrum in the amide I region of PGA_{PAA} indicates that there must be structural rearrangements in the film upon the PAA→PGA exchange.

To reveal the changes in the secondary structure of the PEI-$(PAA/PLL)_5$-[PAA+*PGA*] film, we have tried the following approach: At first, we fitted separately both PAA_{PEI} and PGA_{PEI} with a set of Lorentzian components. PAA needed four, PGA five components for fitting the 1500-1690 cm^{-1} region. (The components are listed in **Table 3** the fitted spectra are not shown.)

Then, PGA_{PAA} was fitted with all the nine components of PAA and PGA, but the frequencies and the widths of the components were fixed only the intensities could be changed during the fit. In this case, excellent fit was obtained (see the curve in the interior of the PGA_{PAA} spectrum, open squares in **Figure 11C**). All PGA components had positive intensities, and all PAA components had negative intensities in agreement with a PAA→PGA exchange.

The PGA_{comp} and PAA_{comp} are calculated spectra **Figure 11C**). They were obtained by summing up all the PGA- and PAA-related component bands, respectively, which were obtained in the fit of the PGA_{PAA} spectrum. $PGA_{PEI\text{-}scaled}$ and $PAA_{PEI\text{-}scaled}$ spectra are the scaled components of the poor fit (shown in **Figure 11B**) obtained for PGA_{PAA} by the linear combination of PGA_{PEI} and PAA_{PEI} spectra. As it can be seen in **Figure 11C** there is a good agreement between $PGA_{PEI\text{-}scaled}$ and PGA_{comp} spectrum in the COO^- stretching region. In the amide I region, however, the intensities of the 1610 and 1647 cm^{-1} bands are higher in the PGA_{comp} spectrum than in the $PGA_{PEI\text{-}scaled}$ spectrum.

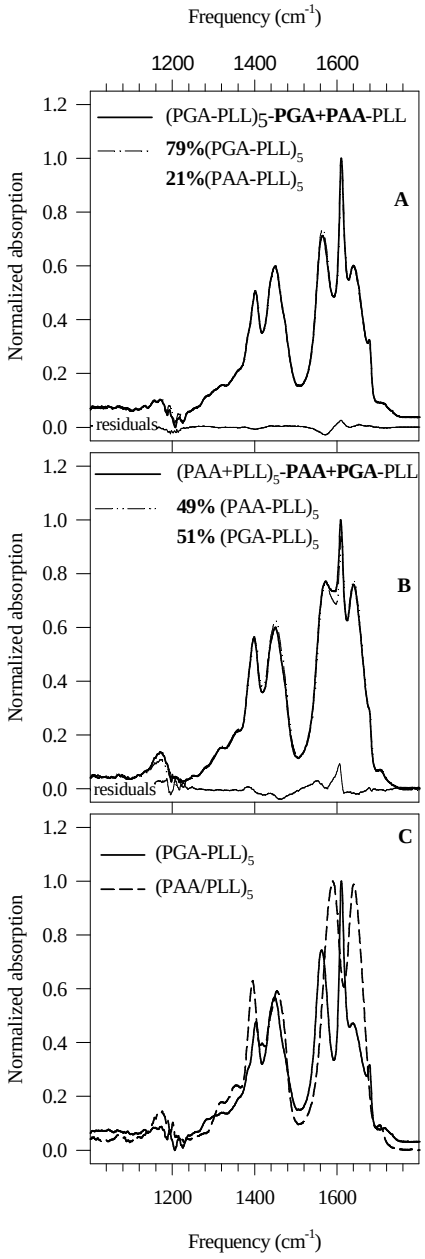

Figure 12: Infrared absorption spectra of 'mixed' (PGA-PLL)$_5$-**PGA+PAA**-PLL (**A**), and (PAA-PLL)$_5$-**PAA+PGA**-PLL (**B**) polyelectrolyte films. The relative amounts of the PGA/PLL and PAA/PLL complexes were determined by fitting with the linear combination of infrared spectra of pure (PGA-PLL)$_5$, and (PAA-PLL)$_5$ films (**C**). The percentages indicate the relative contribution of the given 'pure' film to the structure of the 'mixed' film. For details, see the text.

$PAA_{PEI\text{-}scaled}$ is also similar to PAA_{comp} in the COO^- region. Note, that these spectra have negative amplitudes, since PAA left the polyelectrolyte film upon the exchange with PGA.
In the amide I region, however, according to the PAA_{comp} spectrum, more PAA-related structure is missing than it could be expected on the basis of the $PAA_{PEI\text{-}scaled}$ component. This may mean that the intruding PGA molecules, when they finally incorporate into the existing PAA/PLL architecture force some of the PAA molecules to adopt 'PGA-like' conformations. This more negative amide I region here is the source of the surplus of the PGA-related components with extra intensities in the PGA_{scaled} spectrum shown in the upper part of **Figure 11C**. To compare these mixed films with the pure ones, a terminating PLL layer was added. Thus, (PGA-PLL)$_5$-PGA+PAA-PLL (or (PAA-PLL)$_5$-PAA+PGA-PLL) films were obtained; their infrared absorption spectra are shown in **Figure12A** and **B**, respectively.

One may assume that in these films PGA/PLL and PAA/PLL complexes coexist. If so, the amount of the second polyanion could be estimated by fitting the infrared absorption spectrum of the 'mixed' film with the linear combination of (PGA-PLL)$_5$ and (PAA-PLL)$_5$ spectra. It should be noted here that the infrared spectrum of a pure film is continuously changing as the number of layers is increasing (see **Figure 7**). The five-layered (PGA-PLL)$_5$ and (PAA-PLL)$_5$ films were the closest to the 'mixed' films;

their infrared spectra were used (see **Figure 12C**) in the linear combination fitting.

For $(PGA\text{-}PLL)_5$-PGA+PAA-PLL, the results of the fits are shown in **Figure 12A**. The infrared spectrum could be well fitted with 79% $(PGA\text{-}PLL)_5$ and 21% $(PAA\text{-}PLL)_5$. According to the residuals at the bottom of **Figure 12A**, the fit is rather good, there are some discrepancies only in the amide I region. These values represent the relative amounts of glutamic acid (GA) and aspartic acid (AA) units, and not those of the PGA and PAA polymers since they were obtained after normalizing the spectra used for the fit. The normalization was done by calculating the integrals of $(PGA\text{-}PLL)_5$ and $(PAA\text{-}PLL)_5$ between 1750-1230 cm^{-1}. Believing in the absolute value of this proportion assumes that the extinction coefficients of PGA and PAA are the same. But even if the extinction coefficients were different, changes in the relative amounts would reflect real alterations.

Surprisingly, in $(PAA\text{-}PLL)_5$-PAA+PGA-PLL (**Figure 12B**) there is 49% $(PAA\text{-}PLL)_5$ and 51% $(PGA\text{-}PLL)_5$! Here, the incorporation of PGA is much larger than that of PAA was above in a symmetric situation. The residuals in the amide I region are large (**Figure 12B**, bottom) indicating that the secondary structure of the mixed film is more complex than just the coexistence of unaltered pure $(PGA\text{-}PLL)_5$ and $(PAA\text{-}PLL)_5$ structures.

4.4. Incorporation of a second polyanion to the polyelectrolyte film

HSA as polyelectrolyte film-surface monitor: As it was shown above, PAA and PGA were able to replace each other and incorporate up to a certain extent in/into a polyelectrolyte film. It was not clear, however, whether PGA↔PAA competition involved only the terminal layer, or the interior of the film was also affected. We have seen above that due to the incorporation of the second polyanion PGA/PLL and PAA/PLL domains coexist in the mixed films. Such domains should necessarily be on the surfaces of the films as well. Therefore the infrared spectrum of HSA on the surface of a mixed film should be the linear combination of its spectra on pure films. Since the infrared spectrum of HSA is very different on pure $(PGA\text{-}PLL)_5$ and $(PAA\text{-}PLL)_5$ films there is a chance that the infrared spectrum of HSA adsorbed onto mixed films can be decomposed to component spectra corresponding to pure PAA/PLL and PGA/PLL surface domains. Thus, one may hope to get estimation for the ratio of the two types of domains on the mixed film surface or, more precisely, over the region of the film, which has been affected by the protein adsorption. To test whether such an approach is feasible, the amide I region HSA adsorbed onto a (PGA/PLL)5-PGA+PAA-PLL film

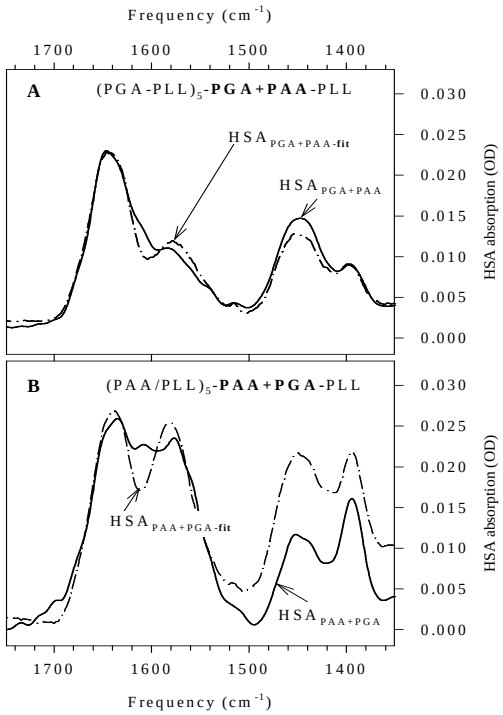

Figure 13: FTIR-ATR spectra of HSA adsorbed onto mixed $(PGA\text{-}PLL)_5$-PGA+PAA-PLL ($HSA_{PGA+PAA}$, panel A), and onto $(PAA\text{-}PLL)_5$-PAA+PGA-PLL ($HSA_{PAA+PGA}$, panel B) polyelectrolyte films. Both HSA spectra were fitted with the linear combination of HSA_{PGA} and HSA_{PAA} (both spectra are shown in **Figure 8**). The fitted spectra are indicated as HSA_{fit} in both panels. The relative amounts of HSA_{PGA} and HSA_{PAA} are given in percentage at the bottom of each panel. The fit was performed between 1685-1525 cm^{-1}, the rest of the fitted spectrum was calculated on the basis of the component weights obtained in the fit

($HSA_{PGA+PAA}$ in **Figure 13A**) was fitted with the linear combination of HSA_{PGA} (shown in **Figure 8A**) and HSA_{PAA} (shown in **Figure 8B**). The fit was quite good, and the relative weights of the HSA_{PGA}=80%, and HSA_{PAA}=20% agreed surprisingly well with the relative weights of PGA/PLL and PAA/PLL in this film (it was 79% and 21%, respectively, as shown above). In contrast, the fit of $HSA_{PAA+PGA}$ with HSA_{PAA} and HSA_{PGA} shown in **Figure13B** is poor, in the amide I region it fails to reproduce the $HSA_{PAA+PGA}$ spectrum, which looks rather strange anyway. (Remember that we see not only the protein in these difference spectra, but also all the changes together, which happened in the system upon the adsorption of the protein.) $HSA_{PAA+PGA}$ exhibits a band characteristic of PGA/PLL complexes at around 1610 cm^{-1}, which is missing from the HSA_{PGA} and HSA_{PAA} spectra. This may indicate additional polyelectrolyte film rearrangement here, upon the adsorption of HSA. In the case of such a systematic deviation between the original and the fitted spectra, it makes no sense to calculate the relative weights of the fitting component spectra.

4.5. Phospholipid model membranes on polyelectrolyte films

4.5.1. DPPC bilayer on the surface of a PGA/PLL polyelectrolyte film

The infrared absorption spectrum of a pure PGA/PLL film was calculated from single beam spectra of PEI and PEI-$(PGA/PLL)_5$-PGA by taking them as background (I_0) and

sample (I), respectively (***OD = -lg(I/I$_0$)***). In **Figure 14**, the C-H stretching region of the infrared spectrum of the PGA/PLL film has less intensive, broad features, while the 1800-1350 cm^{-1} region is showing the strong, characteristic bands of the PGA/PLL complexes, which adopt mostly β-structures.

The infrared absorption spectrum of the DPPC bilayer created on the surface of the polyelectrolyte film was obtained by taking the single beam spectra of PEI-$(PGA/PLL)_5$-PGA as background and that of PEI-$(PGA/PLL)_5$-PGA-DPPC as sample in the calculation. Upon circulating DPPC liposomes above the polyelectrolyte film, and going above the gel→liquid crystalline phase-transition temperature the liposomes 'melt' into a continuous bilayer, thus more lipid molecules were in the depth accessible for the evanescent light. Therefore, the bands related to DPPC molecules became more intensive in the infrared absorption spectrum. In **Figure 14**, the presence of DPPC on the film surface is evident from the characteristic $\nu_{sym}CH_2$ band at around 2850 cm^{-1}, the $\nu_{as}CH_2$ band at around 2920 cm^{-1}, and the corresponding $\nu_{sym}CH_3$ and $\nu_{as}CH_3$ modes at around 2872 and 2958 cm^{-1}, respectively. The low $\nu_{sym}CH_2$ frequency (≈ 2850 cm^{-1}) is indicative of ordered fatty-acyl chains being in gel phase [24,25]. In the infrared spectrum of the DPPC bilayer we measure not only the

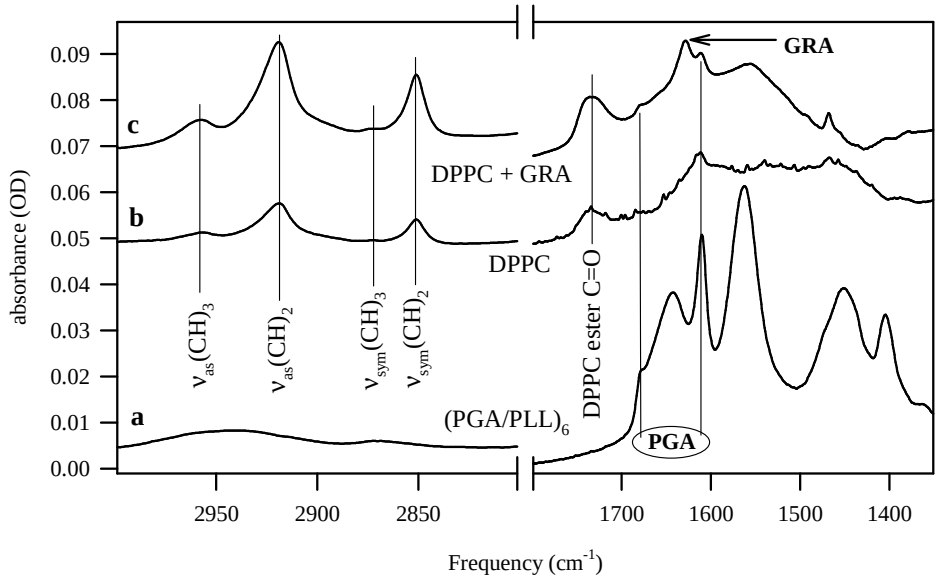

Figure 14: C-H stretching, amide I and II regions of the Fourier transform infrared spectra of a polyelectrolyte film PEI-$(PGA/PLL)_5$-PGA – (**curve a**), of a dipalmitoylphosphatidylcholine bilayer built onto a polyelectrolyte film (DPPC) – (**curve b**), and of DPPC bilayer containing gramicidin A also on the top of a polyelectrolyte film (DPPC+GRA) – (**curve c**).

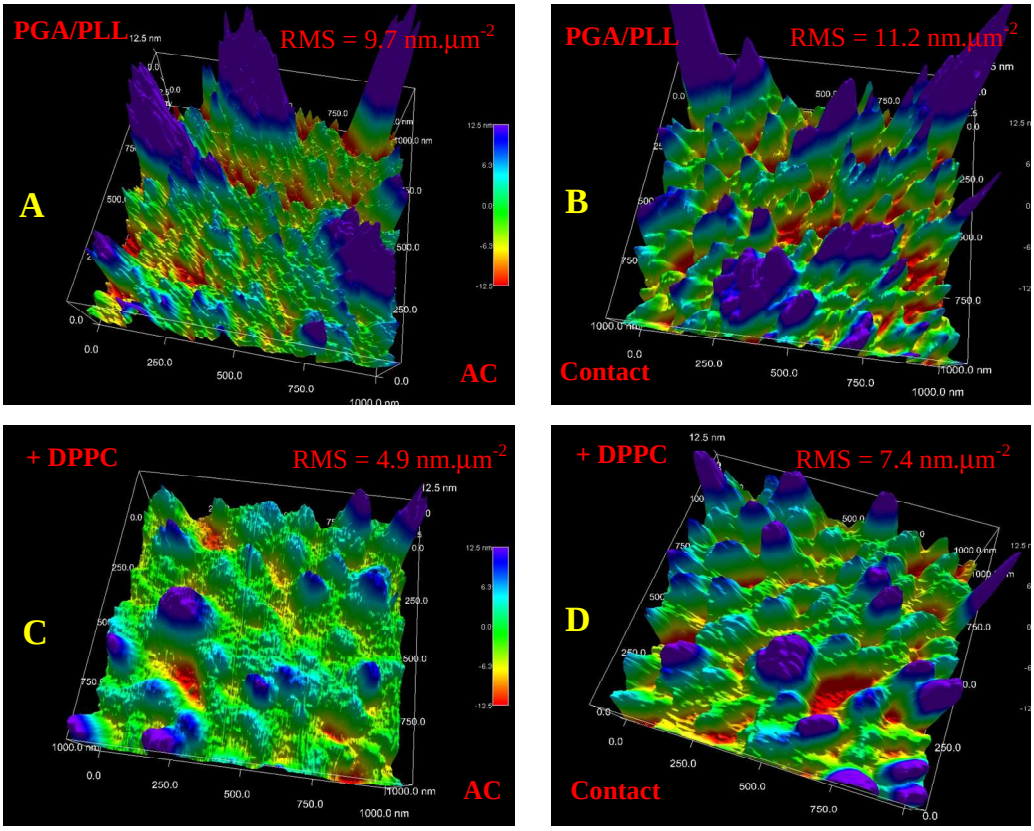

Figure 15: Atomic force microscopic images of pure PEI-(PGA/PLL)$_5$-PGA polyelectrolyte film surfaces (panels A and B), and these films covered with a DPPC bilayer (panels C and D). The left panels show pictures obtained in AC mode, the rights were obtained in contact mode. Note, that upon covering the polyelectrolyte films with DPPC, surface roughness decreased considerably, and the shape of the extruding features also became smoother. Root Mean Squared (RMS) roughness for each sample is given in the panels.

contribution of the DPPC molecules, but also any additional changes, which might appeared upon the formation of the lipid bilayer. Therefore, the weak features corresponding to characteristic PGA/PLL bands in the DPPC spectrum in **Figure 14** indicate small rearrangements in the underlying PGA/PLL film.

Atomic force microscopic measurements have shown (**Figure 15**) that surface roughness of the PGA/PLL films was considerably decreased when they were covered with a DPPC bilayer. In addition, the extruding features became smoother, more 'round' on the DPPC-covered films. It seems that the forces, which keep the DPPC bilayer together, in order to optimise the bilayer structure, can compress the extruding parts of the PGA/PLL films.

4.5.2. The barrier properties of the embedded DPPC bilayer

The DPPC bilayer may represent a barrier at very different levels starting from the large polyelectrolyte molecules down to individual ions. First, we tested its barrier properties against the polyelectrolyte molecules. It has been shown earlier with Optical Waveguide Light-Mode Spectroscopy (OWLS) that PGA/PLL films exhibit exponential growth [16]. Exponential growth can be followed with infrared spectroscopy as well, by recording the infrared spectra after the adsorption of each polyelectrolyte layer, as we have showed above (**Figure 7**).

If the DPPC bilayer represent a barrier, indeed for the polyelectrolyte molecules then a new growth regime should start on the DPPC surface, when additional polyelectrolyte layers are adsorbed. The result of such an experiment is shown in **Figure 16**. Here the increasing absorption of the lower set of infrared spectra shows that, the PGA/PLL film at the beginning was growing exponentially. Reaching the PEI-$(PGA/PLL)_5$-PGA architecture, a DPPC bilayer was created on the film surface. The upper set of infrared spectra in **Figure 16** shows the growth of the additional PGA/PLL layers deposited onto the DPPC-covered film up to the $(PGA/PLL)_6$ architecture. As it can be seen, a new growth regime started on the top of the DPPC bilayer. The question remains, however, what is the nature of the new growth regime, exponential or linear? In **Figure 17** the detailed analysis of the intensities of the infrared spectra of the polyelectrolyte layers adsorbed onto the DPPC bilayer are shown.

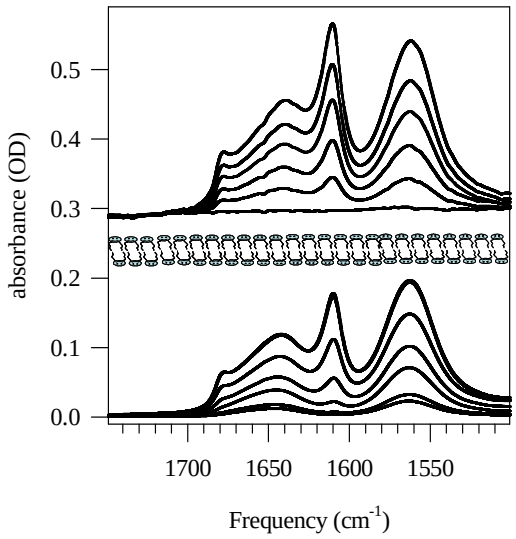

Figure 16: Two separated growth regime of the PGA/PLL film under and above the DPPC bilayer. Lower set of spectra shows the first six PGA layers in the PEI-$(PGA/PLL)_5$-PGA architecture. The DPPC bilayer is schematically represented. Above the schematically depicted DPPC bilayer, the infrared spectra of the other six PGA layers in the $(PGA/PLL)_6$ architecture, built upon the lipid-covered surface, are shown. These spectra were displaced upward for clarity and of didactic reasons

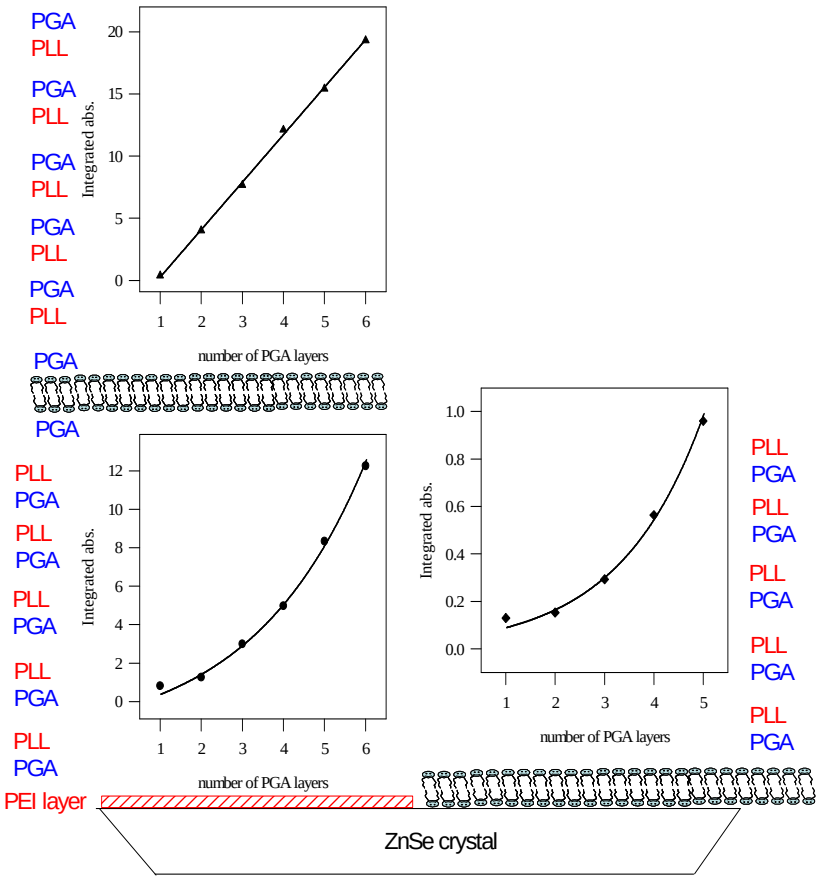

Figure 17: Growth rates of the PGA/PLL multilayers

On the left part of the figure (**Figure 17**) the film architecture is shown, where first the ZnSe crystal was treated with PEI, then five PGA/PLL double layers were adsorbed. The exponential growth rate of this film is shown in the lower left panel. The integrated absorption of the PGA/PLL infrared spectrum between 1700-1500 cm^{-1} was plotted as a function of the number of the PGA layers. The continuous line is the fitted exponential. Then a DPPC bilayer was formed. On the top of the DPPC bilayer first a PGA layer was adsorbed, then five PLL/PGA double layers. The integrated absorption intensities of these PGA/PLL layers are plotted in the upper left panel. As it can be seen, the growth restarted on the top of the DPPC bilayer, but the rate was only linear as shown by the fitted straight line. As a control, on the right side of the figure an experiment is shown, where first a DPPC bilayer was formed on the surface of the bare ZnSe crystal. Then, on the top of the DPPC

bilayer, six PGA/PLL double layers were adsorbed. The growth rate here is clearly exponential, i.e. it is not the lipid surface, which could somehow affect the nature of the growth rate. (The linear growth might be worth of further studies. The problem is that having the DPPC bilayer with different refractive index in between the two polyelectrolyte film makes the system optically rather complex, and the effect of this situation on the propagation of the evanescent wave has to be understood before any other conclusion is made.)

Nevertheless, re-starting growth of the polyelectrolyte film means that the DPPC bilayer represents such a barrier in the PGA/PLL film, which does not allow the diffusion of any polyelectrolyte from one compartment to the other. In contrast to Delajon et al. [56] who could deposit only one additional poly(sodium 4-styrenesulphonate)/poly(allylamine hydrochloride) (PSS/PAH) film on top of their DMPC bilayer, we could deposit six PGA/PLL double layers on top of the lipid bilayer without any sign of problem concerning the adsorption of further layers. The difference between the PSS/PAH and PGA/PLL films may well be related to their different structures, and their different hydrations.

4.5.3. Dynamics and phase properties of the adsorbed/embedded DPPC bilayer

If the DPPC layer is a barrier at least at the polyelectrolyte level as it is expected from a lipid membrane, how its phase properties and dynamics are related to that of lipids in other model membrane systems?

First, as a reference, DPPC bilayer was prepared on bare ZnSe crystal in the same way as on the surface of PGA/PLL films, from circulating liposomes. Its SVD analysis is shown in the upper row of **Figure 18. DPPC-s_1** shows the C-H stretching region of the DPPC infrared spectrum averaged over the whole temperature range studied. **DPPC-s_2** shows the largest change, which, in first approximation, has to be combined with the **DPPC-s_1** to get the originally measured spectra. (In this approximation we neglect the other changes, whose weights are decreasing rapidly.) The shape of **DPPC-s_2** (second panel in the first row of **Figure 18**) agrees with that of obtained for thick, hydrated DPPC multilayers measured with transmission infrared spectroscopy [25]. We have also shown earlier that the $\mathbf{v}_2$ vector belonging to the $\mathbf{s}_2$ basis spectrum describes the gel to liquid crystalline phase transition of DPPC in a perfect agreement with the conventional method based on the temperature-

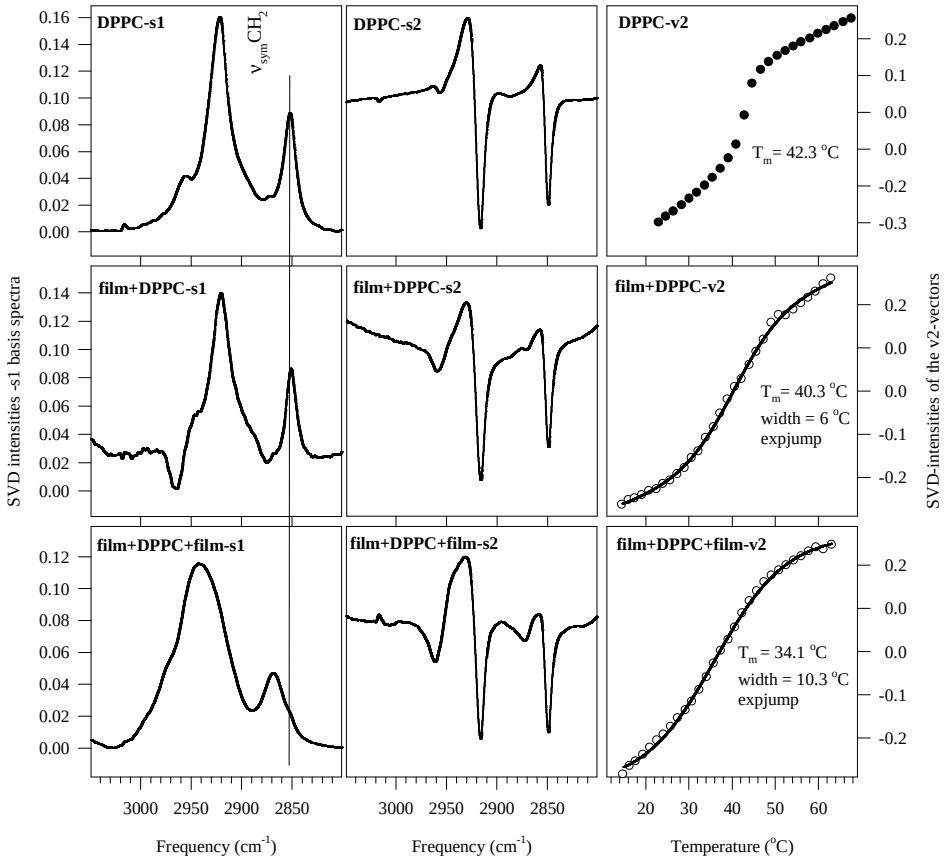

Figure 18: Singular value decomposition (SVD) analysis of DPPC bilayers in different architectures.

induced frequency shift of the $\nu_{sym}CH_2$ band [25]. The third panel of the first row in **Figure 18** shows the temperature dependence of **DPPC-v_2**. Note, that in agreement with the average nature of **DPPC-s_1**, the intensity of **DPPC-v_2** is going from negative to positive having zero intensity around the middle of the change. By interpolating 500 points in between the first and the last measurements using a shifting polynomial of second degree a smooth curve could be obtained. The first derivative of this curve exhibited one sharp maximum at 42.3 °C, which value can be considered as the phase-transition temperature for a pure DPPC bilayer adsorbed onto a bare ZnSe crystal in the presence of D_2O.

When DPPC was layered onto PEI-$(PGA/PLL)_5$-PGA, both its **s_1** and **s_2** basis spectra (**Figure 18**, second row) were very similar to those of DPPC on the bare ZnSe (**Figure 18**, first row). This is not surprising since the infrared absorption spectra of the film-adsorbed DPPC bilayer were calculated from single beam spectra recorded immediately before and

after the adsorption of DPPC onto the film. Nevertheless, if there are changes in the polyelectrolyte film accompanying the DPPC bilayer formation, those will be also present in the $\mathbf{s_1}$, $\mathbf{s_2}$ basis spectra, and in the $\mathbf{v_2}$ vector. Not so much the actual structure, but the temperature dependence of the DPPC bilayer has changed on the surface of the PEI-$(PGA/PLL)_5$-PGA film. This is reflected by the altered temperature dependence of the **film+DPPC-$\mathbf{v_2}$** vector in the last panel of the second row in **Figure 18**. For this curve, the above-mentioned interpolation-derivation method did not provide a narrow, single peak from what the phase transition temperature could be determined. Therefore, to give at least a phenomenological description of the phase transition, we used the function, $y=A/(1+\exp-((x-x_0)/\Gamma))$ (where A is the amplitude, Γ is the width of the transition), which is generally used to characterize transitions from one state to the other; we call it expjump here. Thus, 40.3 °C middle temperature and 6 °C width were obtained for the transition of the **film+DPPC-$\mathbf{v_2}$** vector, which is at somewhat lower temperature and is definitely wider than that of found for the DPPC bilayer on bare ZnSe.

The most challenging task was to determine the lipid-related changes in the case where DPPC was embedded into a PEI-$(PGA/PLL)_5$-PGA-**DPPC**-PGA-$(PLL/PGA)_5$ architecture. Here, the difference spectra, which included the DPPC bilayer, contained also the six PGA layers above the lipid. Therefore, the bands, characteristic for the lipid C-H stretching region, appeared only as shoulders in the **film-DPPC-film-$\mathbf{s_1}$** spectrum (**Figure 18**, third row). Nevertheless, the largest change in this architecture upon increasing temperatures is in the lipid structure, as it can be seen from the large similarity of the **film-DPPC-film-$\mathbf{s_2}$** spectrum to the **DPPC-s2** and **film-DPPC-$\mathbf{s_2}$** spectra. This result shows the power of the SVD analysis to separate individual phenomena from complex processes. The temperature dependence of the phase transition of the embedded DPPC bilayer is shown by **film-DPPC-film-$\mathbf{v_2}$** in the third row of **Figure 18**. This is also a wide transition as in the case of **film-DPPC-$\mathbf{v_2}$** above. Determined with the same two-state function, we obtained T_m=34.1 °C and width=10.3 °C for the temperature and the width of the transition, respectively.

4.5.4. Gramicidin A (GRA) incorporation into the DPPC bilayer

The interaction of GRA with different lipids has already been investigated in details [57]. Here, we first checked the amount of the incorporated peptide among our conditions.

Figure 19A shows the relative intensity of the lipid-related ester C=O and peptide-related amide I bands in a thick sample (dashed line).

This thick sample was obtained by drying from organic DPPC+GRA solution first onto the ZnSe crystal, then the dried layer was hydrated, thus lipid multi-bilayers (dashed line) could be formed. This relative intensity of the GRA amide I band versus the DPPC ester C=O band is similar (precisely: somewhat lower) to that of found for myristoyl-containing lipids [57], i.e. the intensity of the amide I band is considerably higher than that of the ester

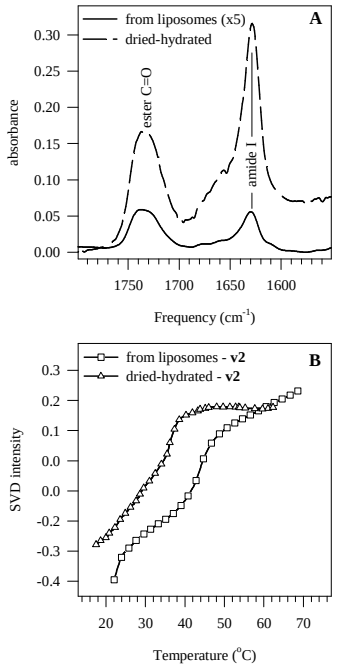

Figure 19: (A **continuous line)** Ester C=O and amide I bands in the infrared absorption spectra of Gramicidin A (GRA) containing DPPC bilayers made from liposomes adsorbed onto the ATR crystal from a circulating suspension. This spectrum is five-times magnified for better visibility; **dashed line** – DPPC+GRA dried onto the ATR crystal by evaporating the organic solvent, and then hydrated. Note, the higher relative intensity of the GRA-related amide I band in the dried-hydrated sample. **B** – **squares** – The $\mathbf{v_2}$ SVD vector calculated from the infrared spectra of GRA-containing DPPC bilayers obtained from adsorbed liposomes. Its phase transition temperature is very similar to that of the pure DPPC bilayer shown in **Figure 18**, the low GRA content little disturbed the DPPC bilayer; **triangles** – The $\mathbf{v_2}$ SVD vector of DPPC+GRA multi-bilayers from dried-hydrated samples. Note that here the phase transition temperature is considerably downshifted.

C=O band. In contrast, in the case of our method, when liposomes were circulating above the crystal surface and only those molecules remained on the surface, which were able to adsorb by themselves, the relative intensity of the amide I band as compared to the ester C=O is much lower (**Figure 19A**, continuous line).

As a consequence, GRA being in a high proportion in the dried-hydrated sample was able to affect considerably the phase transition of DPPC, in contrast to samples obtained directly from circulating liposomes, where the GRA concentration was much lower (**Figure 19B**).

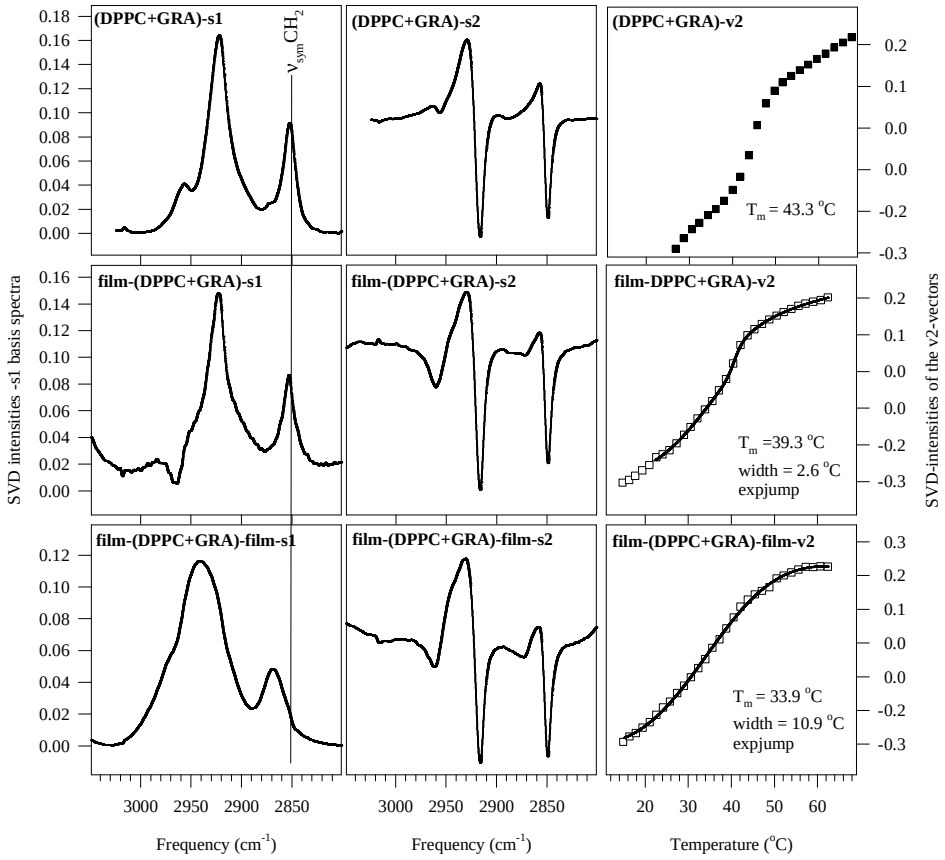

Figure 20: The SVD analysis of Gramicidin A (GRA)-containing DPPC bilayers. According to the spectrum presented in Figure 19, the relative amount of GRA in these bilayers, which were prepared from circulating liposomes, was much lower than the 1:10 molar ratio set in the dried-hydrated samples. The dried-hydrated samples are much thicker and contain lipid multi-bilayers. Note the similarity of both the shapes of the obtained components and their temperature dependence to the curves depicted in **Figure 18** for pure DPPC. Due to its low concentration, GRA was not able to alter measurably the behavior of the DPPC bilayer, created on the polyelectrolyte film surface**.**

These latter one had very similar phase transition to that of the pure DPPC (shown by **DPPC-v_2** in **Figure 18**). This similarity between the behaviour of the DPPC and (DPPC+GRA)-containing cases is persistent in all architectures **Figure 20**.

The characteristic band of GRA is its amide I band at around 1630 cm^{-1}, but due to the large changes of the intensive bands of the PGA/PLL film in the same region, we could not separate the GRA-related alterations even by SVD analysis as a function of the temperature.

Nevertheless, the data show that it is possible to incorporate GRA into the DPPC bilayers, and the GRA molecules remain stably embedded in the lipid environment.

4.6. A preliminary biological essay of the phospholipid bilayer surface on bio-functionalised polyelectrolyte films

Thinking of later possible practical applications, we wanted to check the behaviour of the (polyelectrolyte film+DPPC bilayer) complex among biological conditions. The question was whether the presence of DPPC can modulate the activity of bio-functionalised polyelectrolyte films, where the bio-functionality is membrane-connected. The selected test system was the induction of melanin production in B16F1 melanoma cells. This induction can

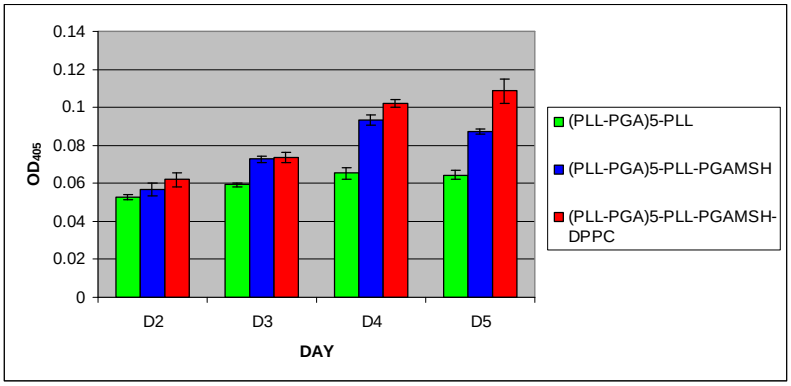

Figure 21: Melanin production in B16-F1 cells in contact with multilayer films containing α-MSH covered by DPPC bilayers. Cells were deposited on multilayer films in 24-well plates at a density of 50.000 cells/well. The amount of the produced melanin was followed by measuring the absorption at 405 nm after 2, 3, 4 and 5 days. The presented data are means of three parallel set of measurements of one experiment and the vertical bars correspond to the standard deviation.

be triggered by a small peptide hormone α-melanocortin (α-MSH: *Ac-Ser-Tyr-Ser-Met-Glu-His-Phe-Arg-Trp-Gly-Lys-Pro-Val-*NH_2). This hormone can induce the melanin production in melanoma cells when added in solution at the concentration of 1 mg/mL [15]. The activity of the α-MSH can be preserved when it is covalently bound to PGA or PLL, and this way it is incorporated into polyelectrolyte films [15,58].

The question was, whether the presence of a DPPC bilayer of the surface of the α-MSH containing PGA/PLL film can modulate the activity of the α-MSH.

Therefore, first, for control we have built $(PLL\text{-}PGA)_6$-PLL multilayer films on glass slides were built. These slides were placed into the wells of 24-well plates, where B16F1 melanoma cells were cultured. In parallel experiments as positive controls $(PLL\text{-}PGA)_5$-PLL-PGA-α-MSH films were used, i.e. these films contained the covalently bound α-MSH. To check the effect of the DPPC bilayer glass plates covered with $(PLL\text{-}PGA)_5$-PLL-PGA-α-MSH+**DPPC** were used. The melanin production was followed by measuring the absorption of the total cell suspension at 405 nm, at a wavelength characteristic of melanin. This is only a first approach, the data are integral type, actually the accommodation of the melanin is followed. The results of such an experiment are shown in **Figure 21**.

It can be seen that over the lifetime of the cells (they died on the 6^{th} day) there was always some stimulating effect of the DPPC on the melanin production. We do not know yet the mechanism of this induction, only speculations can be done, along which further experiments can be designed. One possible reason can be, that DPPC provide better environment for the peptide, which can therefore more effectively interact with the cell membrane. This possibility can be explored by investigating the interaction between DPPC and α-MSH in separate experiments. It also has to be clarified, how the local density of α-MSH in the polyelectrolyte films is related to its concentration in the bulk experiments.

Nevertheless, the first promising results open the way of further investigations concerning the biomedical applications of these DPPC bilayers or other lipid bilayers having lipid compositions tailored to the actual application. The above experiments are only the first, small steps in this direction.

Summary

Following layer-by-layer the build-up of poly-(L-glutamic acid)/poly-(L-lysine) (PGA/PLL) multilayers, we could demonstrate the gradual formation of a strong β secondary structure in the polyelectrolyte films. When the chemically very similar poly-(L-aspartic acid) (PAA) was used as polyanion, the secondary structure of the polypeptide film was markedly different, it contained sizable amount of α-helix, and random structure as well. PGA and PAA could substitute each other in the polyelectrolyte films, but the structural consequences of the substitutions were not symmetrical: While PAA could be incorporated without large effects, the incorporation of PGA into an existing PAA/PLL film caused major structural rearrangement. The different effects can be related to the longer side chain in the glutamic acid, which results looser polyelectrolyte film structure.

We could create a lipid bilayer on the surface of PGA/PLL polyelectrolyte films. In addition, these lipid bilayers could be covered with another polyelectrolyte layers, thus the lipid double layer was embedded into the polyelectrolyte architecture. This system may provide a tool to incorporate lipid-soluble, hydrophobic compounds into the highly charged polyelectrolyte films, which would be important from the point of view of practical applications of such systems. Moreover, such a lipid double layer may be considered as a new model membrane system, where protein-lipid, protein-membrane interactions can be studied. The underlying polypeptide polyelectrolytes provide a large-scale protein-like surface, thus they can mimic the cytoskeleton, the protein network, stabilising the cell membrane.

Finally, we made a first attempt to check, whether such artificial lipid bilayers can affect the activity of biofunctionalised polypeptide surfaces. PGA/PLL films, functionalised by a covalently bound melanocyte-stimulating hormone **(**α-MSH) were covered with lipid double layers. The melanoma cells coming in contact with these surfaces produced somewhat more melanin when the polyelectrolyte architecture contained the lipid double layer as well. These are very preliminary experiments, but they show, that after optimising the lipid composition and the polyelectrolyte architecture for each intended application, such systems might have practical use in solving biomedical problems.

Reference List

1. Williams DF: *The Williams dictionary of Biomaterials.* Liverpool University Press; 1999.

2. Williams DF: **On the mechanisms of biocompatibility.** *Biomaterials* 2008, **29:**2941-2953.

3. Decher G: **Fuzzy nanoassemblies: Toward layered polymeric multicomposites.** *Science* 1997, **277:**1232-1237.

4. Eckle M, Decher G: **Tuning the performance of layer-by-layer assembled organic light emitting diodes by controlling the position of isolating clay barrier sheets.** *Nano Letters* 2001, **1:**45-49.

5. Fou AC, Onitsuka O, Ferreira M, Rubner MF, Hsieh BR: **Fabrication and properties of light-emitting diodes based on self-assembled multilayers of poly(phenylene vinylene).** *Journal of Applied Physics* 1996, **79:**7501-7509.

6. Qiu XP, Leporatti S, Donath E, Mohwald H: **Studies on the drug release properties of polysaccharide multilayers encapsulated ibuprofen microparticles.** *Langmuir* 2001, **17:**5375-5380.

7. Shiratori SS, Rubner MF: **pH-dependent thickness behavior of sequentially adsorbed layers of weak polyelectrolytes.** *Macromolecules* 2000, **33:**4213-4219.

8. Mendelsohn JD, Barrett CJ, Chan VV, Pal AJ, Mayes AM, Rubner MF: **Fabrication of microporous thin films from polyelectrolyte multilayers.** *Langmuir* 2000, **16:**5017-5023.

9. Mendelsohn JD, Yang SY, Hiller J, Hochbaum AI, Rubner MF: **Rational design of cytophilic and cytophobic polyelectrolyte multilayer thin films.** *Biomacromolecules* 2003, **4:**96-106.

10. Zhu YB, Gao CY, He T, Liu XY, Shen JC: **Layer-by-layer assembly to modify poly(L-lactic acid) surface toward improving its cytocompatibility to human endothelial cells.** *Biomacromolecules* 2003, **4:**446-452.

11. Vautier D, Karsten V, Egles C, Chluba J, Schaaf P, Voegel JC, Ogier J: **Polyelectrolyte multilayer films modulate cytoskeletal organization in chondrosarcoma cells.** *Journal of Biomaterials Science-Polymer Edition* 2002, **13:**713-732.

12. Tryoen-Toth P, Vautier D, Haikel Y, Voegel JC, Schaaf P, Chluba J, Ogier J: **Viability, adhesion, and bone phenotype of osteoblast-like cells on polyelectrolyte multilayer films.** *Journal of Biomedical Materials Research* 2002, **60:**657-667.

13. Richert L, Lavalle P, Vautier D, Senger B, Stoltz JF, Schaaf P, Voegel JC, Picart C: **Cell interactions with polyelectrolyte multilayer films.** *Biomacromolecules* 2002, **3:**1170-1178.

14. Boura C, Menu P, Payan E, Picart C, Voegel JC, Muller S, Stoltz JF: **Endothelial cells grown on thin polyelectrolyte mutlilayered films: an evaluation of a new versatile surface modification.** *Biomaterials* 2003, **24:**3521-3530.

15. Chluba J, Voegel JC, Decher G, Erbacher P, Schaaf P, Ogier J: **Peptide hormone covalently bound to polyelectrolytes and embedded into multilayer architectures conserving full biological activity.** *Biomacromolecules* 2001, **2:**800-805.

16. Gergely C, Bahi S, Szalontai B, Flores H, Schaaf P, Voegel JC, Cuisinier FJG: **Human serum albumin self-assembly on weak polyelectrolyte multilayer films structurally modified by pH changes.** *Langmuir* 2004, **20:**5575-5582.

17. Boulmedais F, Frisch B, Etienne O, Lavalle P, Picart C, Ogier J, Voegel JC, Schaaf P, Egles C: **Polyelectrolyte multilayer films with pegylated polypeptides as a new type of anti-microbial protection for biomaterials.** *Biomaterials* 2004, **25:**2003-2011.

18. Hubsch E, Fleith G, Fatisson J, Labbe P, Voegel JC, Schaaf P, Ball V: **Multivalent ion/polyelectrolyte exchange processes in exponentially growing multilayers.** *Langmuir* 2005, **21:**3664-3669.

19. Picart C, Lavalle P, Hubert P, Cuisinier FJG, Decher G, Schaaf P, Voegel JC: **Buildup mechanism for poly(L-lysine)/hyaluronic acid films onto a solid surface.** *Langmuir* 2001, **17:**7414-7424.

20. Elbert DL, Herbert CB, Hubbell JA: **Thin polymer layers formed by polyelectrolyte multilayer techniques on biological surfaces.** *Langmuir* 1999, **15:**5355-5362.

21. Halthur TJ, Elofsson UM: **Multilayers of charged polypeptides as studied by in situ ellipsometry and quartz crystal microbalance with dissipation.** *Langmuir* 2004, **20:**1739-1745.

22. Richert L, Arntz Y, Schaaf P, Voegel JC, Picart C: **pH dependent growth of poly(L-lysine)/poly(L-glutamic) acid multilayer films and their cell adhesion properties.** *Surface Science* 2004, **570:**13-29.

23. Lavalle P, Gergely C, Cuisinier FJG, Decher G, Schaaf P, Voegel JC, Picart C: **Comparison of the structure of polyelectrolyte multilayer films exhibiting a linear and an exponential growth regime: An in situ atomic force microscopy study.** *Macromolecules* 2002, **35:**4458-4465.

24. Casal HL, Mantsch HH: **Polymorphic Phase-Behavior of Phospholipid-Membranes Studied by Infrared-Spectroscopy.** *Biochimica et Biophysica Acta* 1984, **779:**381-401.

25. Kota Z, Debreczeny M, Szalontai B: **Separable contributions of ordered and disordered lipid fatty acyl chain segments to nu CH2 bands in model and biological membranes: A fourier transform infrared spectroscopic study.** *Biospectroscopy* 1999, **5:**169-178.

26. Mendelsohn R, Moore DJ: **Vibrational spectroscopic studies of lipid domains in biomembranes and model systems.** *Chemistry and Physics of Lipids* 1998, **96:**141-157.

27. Szalontai B, Nishiyama Y, Gombos Z, Murata N: **Membrane dynamics as seen by Fourier transform infrared spectroscopy in a cyanobacterium, Synechocystis PCC 6803 - The effects of lipid unsaturation and the protein-to-lipid ratio.** *Biochimica et Biophysica Acta-Biomembranes* 2000, **1509:**409-419.

28. Szalontai B, Kota Z, Nonaka H, Murata N: **Structural consequences of genetically engineered saturation of the fatty acids of phosphatidylglycerol in tobacco thylakoid membranes. An FTIR study 7.** *Biochemistry* 2003, **42:**4292-4299.

29. Arrondo JLR, Goni FM, Macarulla JM: **Infrared-Spectroscopy of Phosphatidylcholines in Aqueous Suspension - A Study of the Phosphate Group Vibrations.** *Biochimica et Biophysica Acta* 1984, **794:**165-168.

30. Bellamy LJ, Chapman and Hall: *The Infrared Spectra of Complex Molecules.* 1980.

31. Mendelsohn RMHH. **Fourier transform infrared studies of lipid-protein interaction.** ***In* Progress in Protein-Lipid Interactions.** 2, 103-146. 1986.

32. Flach CR, Mendelsohn R: **A New Infrared Spectroscopic Marker for Cochleate Phases in Phosphatidylserine-Containing Model Membranes.** *Biophysical Journal* 1993, **64:**1113-1121.

33. Sunder S, Cameron DG, Casal HL, Boulanger Y, Mantsch HH: **Infrared and Raman-Spectra of Specifically Deuterated 1,2-Dipalmitoyl-Sn-Glycero-3-Phosphocholines.** *Chemistry and Physics of Lipids* 1981, **28:**137-147.

34. Mantsch HH, Mcelhaney RN: **Phospholipid Phase-Transitions in Model and Biological-Membranes As Studied by Infrared-Spectroscopy.** *Chemistry and Physics of Lipids* 1991, **57:**213-226.

35. Mantsch HH: **Biological Applications of Fourier-Transform Infrared-Spectroscopy - A Study of Phase-Transitions in Biomembranes.** *Journal of Molecular Structure* 1984, **113:**201-212.

36. Tamm LK, Tatulian SA: **Infrared spectroscopy of proteins and peptides in lipid bilayers 2.** *Quarterly Reviews of Biophysics* 1997, **30:**365-429.

37. Barth A, Zscherp C. **What vibrations tell us about proteins.** *35*, 369-430. 2002.

38. Arrondo JLR, Muga A, Castresana J, Goni FM: **Quantitative Studies of the Structure of Proteins in Solution by Fourier-Transform Infrared-Spectroscopy 5.** *Progress in Biophysics & Molecular Biology* 1993, **59:**23-56.

39. Choi JH, Ham S, Cho M. **Inter-peptide interaction and delocalization of amide I vibrational excitons in myoglobin and flavodoxin.** *117*, 6821-6832. 2002.

40. Chung HS, Tokmakoff A. **Visualization and characterization of the infrared active amide I vibrations of proteins.** *110*, 2888-2898. 2006.

41. Torii H, Tasumi M. **Application of the three-dimensional doorway-state theory to analyse the Amide-I infrared and of globular proteins.** *97*, 92-98. 1992.

42. Eberle AN: *The melanotropins: chemistry, physiology and mechanims of action.* 1988.

43. Henry ER, Hofrichter J: **Singular Value Decomposition - Application to Analysis of Experimental-Data.** *Methods in Enzymology* 1992, **210:**129-192.

44. Butt HJ, Jaschke M: **Calculation of Thermal Noise in Atomic-Force Microscopy.** *Nanotechnology* 1995, **6:**1-7.

45. Florin EL, Rief M, Lehmann H, Ludwig M, Dornmair C, Moy VT, Gaub HE: **Sensing Specific Molecular-Interactions with the Atomic-Force Microscope.** *Biosensors & Bioelectronics* 1995, **10:**895-901.

46. Hutter JL, Bechhoefer J: **Calibration of Atomic-Force Microscope Tips.** *Review of Scientific Instruments* 1993, **64:**3342.

47. Hoh JH, Schoenenberger CA: **Surface-Morphology and Mechanical-Properties of Mdck Monolayers by Atomic-Force Microscopy 4.** *Journal of Cell Science* 1994, **107:**1105-1114.

48. Boulmedais F, Schwinte P, Gergely C, Voegel JC, Schaaf P: **Secondary structure of polypeptide multilayer films: An example of locally ordered polyelectrolyte multilayers.** *Langmuir* 2002, **18:**4523-4525.

49. Susi H, Timasheff SN, tevens L: **Infrared Spectra and Protein Conformations in Aqueous Solutions. I. THE AMIDE I BAND IN H2O AND D2O SOLUTIONS.** *J Biol Chem* 1967, **242:**5460-5466.

50. van Stokkum IH, Linsdell H, Hadden JM, Haris PI, Chapman D, and Bloemendal M: **Temperature-Induced Changes in Protein Structures Studied by Fourier Transform Infrared Spectroscopy and Global Analysis.** *Biochemistry* 1995, **34:**10508-10518.

51. Jackson M, Haris PI, Chapman D: **Conformational transitions in poly(L -lysine): studies using Fourier transform infrared spectroscopy.** *Biochim Biophys Acta* 1989, **998:**75-79.

52. Boulmedais F, Bozonnet M, Schwinte P, Voegel JC, Schaaf P: **Multilayered polypeptide films: Secondary structures and effect of various stresses 2.** *Langmuir* 2003, **19:**9873-9882.

53. Schwinte P, Voegel JC, Picart C, Haikel Y, Schaaf P, Szalontai B: **Stabilizing effects of various polyelectrolyte multilayer films on the structure of adsorbed/embedded fibrinogen molecules: An ATR-FTIR study.** *Journal of Physical Chemistry B* 2001, **105:**11906-11916.

54. Schwinte P, Ball V, Szalontai B, Haikel Y, Voegel JC, Schaaf P: **Secondary structure of proteins adsorbed onto or embedded in polyelectrolyte multilayers.** *Biomacromolecules* 2002, **3:**1135-1143.

55. Debreczeny M, Ball V, Boulmedais F, Szalontai B, Voegel JC, Schaaf P: **Multilayers built from two component polyanions and single component polycation solutions: A way to engineer films with desired secondary structure 1.** *Journal of Physical Chemistry B* 2003, **107:**12734-12739.

56. Delajon C, Gutberlet T, Steitz R, Mohwald H, Krastev R: **Formation of poly,electrolyte multilayer architectures with embedded DMPC studied in situ by neutron reflectometry.** *Langmuir* 2005, **21:**8509-8514.

57. Kota Z, Pali T, Marsh D: **Orientation and lipid-peptide interactions of gramicidin A in lipid membranes: Polarized attenuated total reflection infrared spectroscopy and spin-label electron spin resonance 1.** *Biophysical Journal* 2004, **86:**1521-1531.

58. Schultz P, Vautier D, Richert L, Jessel N, Haikel Y, Schaaf P, Voegel JC, Ogier J, Debry C: **Polyelectrolyte multilayers functionalized by a synthetic analogue of an anti-inflammatory peptide, alpha-MSH, for coating a tracheal prosthesis.** *Biomaterials* 2005, **26:**2621-2630.